Title

Oncogenic KRAS Regulates Amino Acid Homeostasis and Asparagine Biosynthesis via ATF4 and Alters Sensitivity to L-Asparaginase

Journal

Cancer Cell, 33(1)

ISSN

1535-6108

Authors

Gwinn, Dana M
Lee, Alex G
Briones-Martin-del-Campo, Marcela
et al.

Publication Date

2018

DOI

10.1016/j.ccell.2017.12.003

Peer reviewed

HHS Public Access

Author manuscript

Cancer Cell. Author manuscript; available in PMC 2019 January 08.

Published in final edited form as:

Cancer Cell. 2018 January 08; 33(1): 91–107.e6. doi:10.1016/j.ccell.2017.12.003.

Oncogenic KRAS regulates amino acid homeostasis and asparagine biosynthesis via ATF4 and alters sensitivity to L-asparaginase

Dana M. Gwinn[1,4], **Alex G. Lee**[1,4], **Marcela Briones-Martin-del-Campo**[4], **Crystal S. Conn**[2], **David R. Simpson**[1,4], **Anna I. Scott**[3], **Anthony Le**[3], **Tina M. Cowan**[3], **Davide Ruggero**[2], and **E. Alejandro Sweet-Cordero**[1,4,‡]

[1]Division of Hematology and Oncology, Department of Pediatrics, Stanford University School of Medicine, Stanford, CA 94305, USA

[2]School of Medicine and Department of Urology, Helen Diller Family Comprehensive Cancer Center, University of California, San Francisco, San Francisco, CA 94158, USA

[3]Stanford University Department of Pathology. Stanford, CA 94305, USA

Summary

KRAS is a regulator of the nutrient stress response in non-small cell lung cancer (NSCLC). Induction of the ATF4 pathway during nutrient depletion requires AKT and NRF2 downstream of KRAS. The tumor suppressor KEAP1 strongly influences the outcome of activation of this pathway during nutrient stress; loss of KEAP1 in KRAS mutant cells leads to apoptosis. Through ATF4 regulation, KRAS alters amino acid uptake and asparagine biosynthesis. The ATF4 target asparagine synthetase (ASNS) contributes to apoptotic suppression, protein biosynthesis and mTORC1 activation. Inhibition of AKT suppressed ASNS expression, and combined with depletion of extracellular asparagine, decreased tumor growth. Therefore, KRAS is important for the cellular response to nutrient stress, and ASNS represents a promising therapeutic target in KRAS mutant NSCLC.

eTOC Blurb

Gwinn et al. show that oncogenic KRAS regulates amino acid homeostasis and cellular response to nutrient stress via ATF4. They identify ASNS as a key target of the KRAS-ATF4 axis in KRAS-driven non-small cell lung cancer, revealing a therapeutic vulnerability in asparagine biosynthesis.

Correspondence to: E. Alejandro Sweet-Cordero: Alejandro.Sweet-Cordero@ucsf.edu, Current address: 1550 4th street. Rock Hall Room 384D. University of California San Francisco, 94158.

[4]Current affiliation: Division of Hematology and Oncology, Department of Pediatrics, University of California San Francisco, San Francisco, CA 94158, USA

‡Lead Contact

Author contributions

Conceptualization: D.M.G. and E.A.S.C.; Methodology: D.M.G., T.M.C., D.R., E.A.S.C., and; Investigation: D.M.G., A.G.L., M.B.M.C, C.S.C, D.R.S., A.I.S., A.L.; Writing: –Original Draft: D.M.G. and E.A.S.C. Writing–Review & Editing: D.M.G., D.R.S. and E.A.S.C.; Funding Acquisition: D.M.G. and E.A.S.C.; Resources; D.M.G. and E.A.S.C.; Supervision: D.M.G. and E.A.S.C.

Introduction

Ras family small GTPases are involved in transmission of extracellular mitogenic stimuli. Ras mutations activate proliferation and survival pathways including RAF-MEK-ERK and PI3K-AKT (Schubbert et al., 2007). Despite their prevalence, no effective Ras-targeted therapies exist. KRAS is mutated in approximately 30% of non-small cell lung cancer (NSCLC) (TCGA, 2014). Understanding how KRAS drives lung cancer pathogenesis and finding targetable vulnerabilities is a major priority for cancer research.

Cancer cells must acquire macromolecular precursors including amino acids, nucleic acids and fatty acids to sustain growth (Vander Heiden et al., 2008). The corresponding biosynthetic pathways are frequently up-regulated in tumors, often by the same oncogenes that drive proliferation (Levine and Puzio-Kuter, 2010). Several biosynthetic pathways are fueled by glutamine, which acts as the primary nitrogen donor for nucleotide and non-essential amino acid synthesis, replenishes TCA cycle intermediates, and maintains redox balance through glutathione (GSH) production (DeBerardinis et al., 2008). Due to insufficient vascularization, tumors are often nutrient depleted (Hensley et al., 2013). How oncogenes regulate the response to limited nutrient availability is not well understood.

Previous work has implicated KRAS as a regulator of several metabolic pathways (Bryant et al., 2014), but little is known about the role of KRAS in metabolic reprogramming in NSCLC. In pancreatic cancer, KRAS alters glutamine metabolism via GOT1 to enhance NADPH production (Son et al., 2013) and up-regulates macropinocytosis to enhance nutrient uptake (Commisso et al., 2013). Our current understanding of the role of KRAS in tumor metabolism is derived largely from studies using supra-physiologic levels of nutrients including glutamine. Such approaches cannot fully interrogate how oncogenes function under the conditions of limited nutrient availability characteristic of in vivo tumor growth. Using both in vitro and in vivo approaches, we set out to investigate the role of oncogenic KRAS under conditions of nutrient deprivation.

RESULTS

Response to KRAS knockdown is influenced by nutrient status

Tumor cells experience fluctuating nutrient availability. To define how KRAS influences response to nutrient stress, we knocked-down KRAS in a genetically diverse panel of NSCLC cell lines (Figure 1A and S1A). Cells were cultured in standard (4mM) or low (0.5mM) glutamine, which more closely reflects plasma glutamine levels (Le et al., 2014). In high glutamine, KRAS knock-down suppressed proliferation (Figure S1B). In low glutamine, cells proliferated at a slower rate, and KRAS knockdown led to a small but statistically significant further reduction in proliferation (Figure S1B). In two of four cell lines tested, low glutamine induced apoptosis (Figure 1B), which was rescued by KRAS knockdown (Figure 1B). We explore the mechanism of this KRAS-specific sensitivity to apoptosis in low glutamine below.

Gene expression analysis identified 495 genes altered by glutamine deprivation (222 up-, 273 down-regulated, fold change (FC) >1.4) (Figure 1C and Tables S1, S2). Genes up-regulated in low glutamine were enriched for the unfolded protein response and ER stress pathways, while cholesterol biosynthesis and cell cycle related pathways were enriched among down-regulated genes (Figure S1C). KRAS knockdown altered 265 genes in high glutamine (117 up-, 148 down-regulated, FC>1.4, Figure 1D and Table S1, S2), with enrichment in cell-cycle-related genes (Figure S1D). In low glutamine KRAS regulated a larger set of 502 genes (204 up-, 298 down-regulated, FC>1.4, Figure 1E and Tables S1, S2), indicating that KRAS regulates distinct sets of genes depending on the nutrient status of cells. 100 genes had altered expression in response to both glutamine deprivation and KRAS knockdown in low glutamine (Figure 1F). In this gene set, all genes up-regulated in glutamine deprivation were suppressed by KRAS knockdown (n=65) (Figure 1G). Thus, KRAS signaling supports a specific transcriptional program in response to glutamine deprivation. Pathway analysis of genes regulated by glutamine deprivation, by KRAS in low glutamine, or both indicated enrichments in the unfolded protein response (UPR), ER stress pathway, serine biosynthesis, folate transformations, tRNA charging, and asparagine biosynthesis (Figure 1H).

Analysis of the 100 genes with altered expression in both glutamine deprivation and KRAS knockdown in low glutamine using a public lung cancer gene expression dataset revealed that tumors with high expression of these genes had lower survival (Figure 1I, Cox hazard ratio = 1.75), an effect which was more pronounced in KRAS mutant tumors (Figure 1J, Cox hazard ratio=2.42). Therefore, response to KRAS knockdown is dependent on nutrient status and the regulation of glutamine response genes by KRAS has prognostic implications for lung cancer patients.

KRAS signaling cooperates with the GCN2-p-eIF2 pathway to induce ATF4

To identify transcription factors responsible for driving gene expression during glutamine deprivation and in response to KRAS signaling in low glutamine, we searched for common binding motifs near the transcriptional start site (TSS) of the 100 genes regulated by both conditions. This revealed enrichment for ATF4 binding sites (Figure 2A)(CREB binding elements were identical to ATF4 binding sites). To corroborate the presence of ATF4 binding sites in this gene set, we compared it to previously published ATF4 ChIP-seq data (Han et al., 2013; Wang et al., 2015). 39/100 genes regulated by KRAS in low glutamine and by glutamine deprivation also had ATF4 binding in their promoters (Figure S2A), including canonical ATF4 targets *ASNS*, *TRIB3*, *DDIT3* (CHOP), *PPP1R15A* (GADD34), and *ATF3*. Therefore, KRAS regulates the response to nutrient stress at least in part through altering the activity of ATF4.

ATF4 is a critical effector during nutrient deprivation (Ameri and Harris, 2008), and regulates many of the same pathways regulated by KRAS (Harding et al., 2003; Ye et al., 2012), suggesting that ATF4 is a regulator of the transcriptional output of KRAS during glutamine deprivation. Consistently, ATF4 target genes *ASNS*, *TRIB3*, *CHOP*, *GADD34*, and *ATF3* all displayed KRAS-dependent mRNA induction in low glutamine (Figure 2B), and KRAS knockdown suppressed protein levels of ATF4 and ASNS in low glutamine

(Figure 2C). As KRAS knockdown suppresses proliferation, it is possible that glutamine consumption decreases proportionally such that low glutamine is sufficient to support growth. However, induction of ATF4 and its targets are dependent on KRAS throughout a time-course of complete glutamine withdrawal (Figure S2B, S2C). Thus, differential proliferative rates and glutamine consumption do not account for the KRAS-dependent disparity in ATF4 induction. In normal lung epithelial cells, ATF4 targets are up-regulated 2–6 fold during glutamine deprivation while in KRAS mutant tumor cells activation was dramatically enhanced (10–50 fold) (Figure S2D).

In nutrient replete conditions, two uORFs in ATF4 engage the ribosomal machinery, preventing translation of the protein-coding ORF, resulting in low levels of ATF4 protein (Vattem and Wek, 2004). eIF2 is phosphorylated by GCN2 during amino acid stress (Castilho et al., 2014), or by PERK during ER stress (Donnelly et al., 2013), leading to a deficiency in preinitiation complexes. Phosphorylation of eIF2 suppresses global protein synthesis but allows the 40S ribosomal subunits to scan past the second uORF in *ATF4* before acquiring a new preinitiation complex, thereby engaging the protein-coding ATF4 ORF, and enhancing ATF4 protein levels (Vattem and Wek, 2004). Due to this unique mechanism, it is accepted that ATF4 is primarily regulated post-transcriptionally by phosphorylation of eIF2.

As expected, inhibition of translation blocked induction of ATF4 protein (Figure 2D). However, inhibition of transcription also suppressed ATF4 protein levels (Figure 2D), suggesting a mechanism of ATF4 regulation distinct from the canonical p-eIF2 translational induction. While KRAS knockdown decreased ATF4, it enhanced eIF2 phosphorylation (Figure 2C), indicating that KRAS signaling regulates ATF4 through an alternative mechanism. Indeed, KRAS knockdown altered mRNA levels of ATF4 (Figure 2E). While KRAS altered mRNA levels of ATF4, this cannot up-regulate ATF4 protein expression in the absence of GCN2-mediated eIF2 phosphorylation because the need to disengage the alternative uORF (Figure 2F, G). Thus, under conditions of nutrient stress, the KRAS and GCN2-eIF2 pathways cooperate to regulate ATF4 at both the transcriptional and translational levels.

NRF2 is required for KRAS-mediated regulation of ATF4 via PI3K

To identify KRAS effectors responsible for regulation of ATF4, we used pharmacological inhibitors to block downstream pathways. PI3K (BKM120), AKT (MK2206), MEK (AZD6244), and RSK (BRD7389) inhibition suppressed induction of ATF4 (Figure 3A, B), indicating multiple mechanisms of regulation. RSK phosphorylates ATF4 to protect it from proteasomal degradation (Hao et al., 2016). However, proteasome inhibition suppressed expression of TRIB3 and ASNS (Figure S3A), suggesting this is not the mechanism of KRAS-dependent regulation of ATF4. Rapamycin also had a minimal effect on ATF4 induction, indicating an mTORC1 independent mechanism for KRAS driven ATF4 induction (Figure 3A, B). As both PI3K and AKT inhibition decreased ATF4, we further investigated the role of this pathway in ATF4 regulation. Constitutively active (myristoylated) AKT, but not kinase dead AKT (K179M) rescued ATF4 target gene expression upon KRAS knockdown (Figure 3C, D). We also observed AKT-dependent

regulation of *ATF4* mRNA levels (Figure 3C), suggesting that KRAS regulates ATF4 transcriptionally downstream of AKT. Thus, despite the redundancy in ATF4 regulation suggested by the pharmacological inhibitors, the PI3K pathway is a key regulator of the ability of KRAS to activate ATF4.

The mRNA levels for the transcription factor NRF2 were decreased by KRAS knockdown in low glutamine (Figure S2A). Best characterized as a regulator of oxidative stress and detoxification (Gorrini et al., 2013), NRF2 also up-regulates ATF4 transcriptional activity (Afonyushkin et al., 2010; Dey et al., 2015; He et al., 2001; Miyamoto et al., 2011; Ye et al., 2014). KRAS and its effector pathways have been shown to regulate NRF2 (DeNicola et al., 2011; Jain and Jaiswal, 2007). In NSCLC, knockdown of KRAS or inhibition of PI3K suppressed NRF2 protein levels (Figure 3E, F). Supporting NRF2 as the relevant target of KRAS upstream of ATF4, knockdown of NRF2 attenuated induction of ATF4 and ATF4 targets in low glutamine (Figure 3G, H). NRF2 was required for induction of ATF4 targets even at early time points during glutamine withdrawal (Figure 3I). Thus, transcriptional control of ATF4 by NRF2 is required to support the translational enhancement provided by the GCN2-p-eIF2 pathway. These data clarify the importance of the KRAS-AKT-NRF2-ATF4 axis as an activator of the transcriptional response program induced by glutamine deprivation. In support of this mechanism, analysis of publicly available proteomic data indicates that tumors with higher *ATF4* expression (Figure S3B) have elevated protein levels of NRF2 (Figure 3J) as well as lower levels of KEAP1 (Figure 3K).

Outcome of ATF4 activation is dependent on nutrient status and genetic context

Previous work has suggested both pro- and anti- oncogenic roles for ATF4. Supporting a pro-oncogenic role, ATF4 promotes fibrosarcoma xenograft tumor growth (Ye et al., 2010), and metastasis (Dey et al., 2015), and in NSCLC, ATF4 up-regulates genes correlated with poor prognosis (DeNicola et al., 2015). In contrast, ATF4 inhibits tumor growth in neuroblastoma (Qing et al., 2012) and the ATF4 target gene CHOP promotes apoptosis (Hetz, 2012). We sought to understand when ATF4 plays growth verse apoptotic roles in tumorigenesis.

To elucidate the role of ATF4 in NSCLC in response to nutrient stress, we analyzed the effect of ATF4 loss across a large panel of cell lines in high and low glutamine. In all cell lines, knock-down of ATF4 decreased viability even in high glutamine (Figure 4A, S4A). In low glutamine, the effect of ATF4 knock-down on viability is diminished, and in a subset of cell lines, loss of ATF4 increased viability (Figure 4A). Notably, the protective effect of ATF4 knockdown in low glutamine was seen only in cells lines with KEAP1 loss. KEAP1 status was confirmed as a determinant of the effect of ATF4 activity in low glutamine, as only those cells bearing KEAP1 mutations undergo apoptosis under these conditions (Figure 4B). Knock-down of ATF4 in two KRAS mutant/KEAP1 mutant cell lines established that apoptosis in low glutamine is dependent on ATF4 (Figure 4C). Induction of ATF4 targets is dramatically enhanced in cells bearing KRAS and KEAP1 mutations when compared to cells wild-type for KEAP1 or KRAS (Figure 4D). This suggests a model in which elevated levels of ATF4 targets induce apoptosis, and thus reduce viability during glutamine

deprivation. Indeed, we observe a step-wise decrease in viability during glutamine deprivation according to mutations that alter levels of ATF4 target induction (Figure 4E).

To test whether altering the KEAP1-NRF2 axis would alter sensitivity to nutrient deprivation, KEAP1 was knocked-down in a KEAP1 wild-type cell line, which led to induction of the NRF2 target SLC7A11, confirming enhanced NRF2 activity (Figure 4F). When KEAP1 was suppressed, TRIB3 mRNA (Figure 4F), and ATF4 and ASNS protein levels (Figure 4G) were enhanced in low glutamine. Only cells with KEAP1 suppression, and elevated ATF4 levels induced cleaved PARP in low glutamine, indicating that elevated NRF2-dependent ATF4 expression sensitized cells to apoptosis (Figure 4G). This indicates that the KRAS-dependent apoptosis observed previously (Figure 1B) is due to ATF4 expression. This data demonstrates that regulation of NRF2 by KRAS or KEAP1 mediates the outcome of nutrient stress by altering ATF4 activity.

These results suggest that nutrient stress and the strength of signaling down the KRAS-NRF2-ATF4 axis can lead to apoptosis under certain conditions. We sought to define the role of ATF loss in vivo. CRISPR-Cas9-mediated knockout of ATF4 in a xenograft model revealed that the overall effect of loss of ATF4 was suppression of tumor growth (Figure 4H, I, S4B). This indicates that nutrient levels in vivo are not sufficiently low to induce ATF4-dependent apoptosis. However, taken together these results indicate that ATF4 activation in response to nutrient stress could be exploited for therapeutic benefit.

KRAS regulates amino acid transport and metabolism during nutrient stress

ATF4 regulates genes encoding amino acid transporters and amino acid metabolism (Ameri and Harris, 2008; Harding et al., 2003). Analysis of several amino acid transporters confirmed ATF4- (Figure S5A, S5B), and KRAS-dependent (Figure 5A, B) expression in high and low glutamine, indicating that KRAS-ATF4 may regulate amino acid uptake in both conditions (Figure 5A, B). ATF4 occupancy was enhanced at the promoters of amino acid transporters in glutamine deprivation, similar to the canonical ATF4 target, ASNS (Figure S5C). The KRAS-ATF4 regulated transporters are responsible for uptake of many amino acids (Hyde et al., 2003), indicating that KRAS broadly influences amino acid availability. Uptake of both glutamine and leucine were dependent on ATF4 (Figure S5D, S5E), and KRAS even in 4mM glutamine (Figure 5C, D), consistent with changes in protein levels of amino acid transporters. These results support a role for KRAS in regulating amino acid transport via ATF4.

KRAS-dependent amino acid transporter expression and uptake suggests that intracellular levels of amino acids can be altered by KRAS. Mass spectrometry analysis indicated that intracellular concentrations of essential amino acids present in DMEM (methionine, leucine, isoleucine, lysine, tryptophan, phenylalanine, histidine, arginine) were sustained in cells cultured in low glutamine (Figure 5E). Knockdown of KRAS suppressed levels of essential amino acids in high and low glutamine (Figure 5E). In contrast, concentrations of amino acids dependent on glutamine for biosynthesis and not present in DMEM (aspartate, asparagine, glutamate, and proline) were reduced in cells cultured in low glutamine regardless of KRAS expression (Figure 5E). Glutamine levels were significantly elevated in cells with knockdown of KRAS in high glutamine (Figure 5E). KRAS regulates numerous

glutamine-consuming enzymes including *ASNS* and *GFPT1* (Figure 2B, C, S5F), suggesting that accumulation of glutamine results from down-regulation of these genes. These results identify the importance of KRAS signaling in maintaining amino acid levels and indicate that KRAS influences amino acid uptake through regulation of transporter expression.

KRAS contributes to protein biosynthesis and supports mTORC1 signaling via regulation of ASNS

Induction of ATF4 during glutamine deprivation requires the eIF2 kinase GCN2, which is activated by uncharged tRNAs when amino acids are scarce (Castilho et al., 2014). Glutamine deprivation decreases levels of only certain amino acids, including asparagine (Figure 5E), so its role in suppressing GCN2 may be due specifically to reduction of these amino acids. *De novo* biosynthesis of asparagine is dependent on a single enzyme, asparagine synthetase (ASNS), which transfers the γ amino group of glutamine to aspartate, yielding asparagine and glutamate (Balasubramanian et al., 2013). To test whether asparagine levels played a role in glutamine-deprivation mediated activation of the GCN2-p-eIF2α pathway, exogenous asparagine was added to cells cultured in low glutamine. Up-regulation of ATF4 protein in low glutamine was attenuated by addition of asparagine (Figure 6A). Furthermore, addition of asparagine (Figure 6A) or ASNS-overexpression suppressed ATF4-dependent apoptosis (Figure 6B). This supports reports that asparagine suppresses apoptosis during amino acid deprivation (Ye et al., 2010; Zhang et al., 2014) and uncovers the existence of a feedback loop where low asparagine stimulates GCN2, to activate ATF4 and enhance ASNS expression.

To isolate the effect of asparagine deprivation, we analyzed knockdown of ASNS in high glutamine with or without addition of asparagine. Consistent with a model where asparagine deprivation alone activates GCN2, knockdown of ASNS in the absence of asparagine was sufficient to induce ATF4 (Figure 6C), and to induce apoptosis in KEAP1 mutant cells (Figure 6C). As expected, ASNS was required for growth in the absence of asparagine in the media (Figure S6A). In cells that did not undergo apoptosis in low glutamine, morphological changes (Figure S6B) and cell cycle arrest (Figure S6C) were observed in both high and low glutamine and were rescued by addition of asparagine or over-expression of ASNS (Figure S6D). Together, these results demonstrate that asparagine is required for cellular proliferation, plays a role in regulating the GCN2-p-eIF2 pathway, and suppresses apoptosis induced by nutrient deprivation. Furthermore, consistent with reports (Ye et al., 2010) addition of exogenous asparagine, or overexpression of ASNS rescued the proliferative defect of ATF4 knockdown (Figure 6D). Therefore, ASNS is an important pro-growth target of ATF4.

Asparagine has been suggested to be an ideal gauge for nutrient requirements for protein synthesis (Zhang et al., 2014), and a rate-limiting amino acid for translation (Arnstein et al., 1986). Knockdown of ASNS was sufficient to suppress protein biosynthesis (Figure S6E). Glutamine deprivation also suppressed protein synthesis rates, which were further reduced by ASNS knockdown (Figure S6E). However, addition of asparagine only rescued protein synthesis rates to those of control shGFP cells in low glutamine, indicating that in high glutamine, asparagine is the rate-limiting amino acid for protein synthesis, while in low

glutamine loss of other amino acids contributes to suppressed protein synthesis. Consistent with KRAS dependent regulation of ASNS, KRAS knockdown was sufficient to suppress global protein synthesis, which was completely rescued by exogenous asparagine (Figure 6E) or by overexpression of ASNS (Figure 6F). Rate of translation was measured by incorporation of leucine into peptides, however differential leucine uptake was observed upon KRAS knockdown (Figure 4D). Asparagine did not alter leucine uptake (Figure S6F), demonstrating that the rescue of protein synthesis is not dependent on amino acid uptake. Additionally, KRAS-dependent methionine incorporation was rescued by addition of asparagine (Figure 6G). While KRAS knockdown had a mild suppressive effect (~10%) on methionine uptake (Figure S6G), the effect on methionine incorporation was much greater (~50%). Asparagine rescued KRAS-dependent methionine incorporation, but did not significantly alter uptake (Figure S6G). This demonstrates that supporting asparagine biosynthesis is a key role for KRAS. Through this mechanism, KRAS plays an important role in regulating the pro-oncogenic metabolic reprogramming.

The cellular growth regulator mammalian target of rapamycin complex 1 (mTORC1) coordinates inputs from growth factor signaling and nutrients including amino acids (Zoncu et al., 2011). Asparagine levels have been implicated in regulation of mTORC1 (Krall et al., 2016). Knockdown of ASNS in high glutamine had minimal effect on phosphorylation of S6, a readout of mTORC1 signaling, while in low glutamine, p-S6 was severely depleted upon ASNS knockdown (Figure 6H). This suggests that asparagine biosynthesis plays a key role in KRAS-dependent regulation of mTORC1 during nutrient deprivation. Indeed, KRAS knockdown in high glutamine had a mild suppressive effect on p-S6 whereas in low glutamine, p-S6 was largely dependent on KRAS expression (Figure 6I). Activation of the ERK and AKT pathways downstream of KRAS have been implicated in regulation of mTORC1 (Zoncu et al., 2011). However, these pathways were not differentially regulated in high vs. low glutamine (Figure 6I), and cannot account for the effect of KRAS in low glutamine. Reinforcing a model in which asparagine is critical for KRAS to support mTORC1 signaling during nutrient deprivation, addition of asparagine rescued the suppression of p-S6 observed upon KRAS knockdown in low glutamine (Figure 6J). Despite the complex role of KRAS in altering multiple signaling pathways, these results demonstrate a fundamental role for ASNS as a mediator of the effect of KRAS on the ability of cells to incorporate new biomass through protein synthesis.

Asparagine synthetase is rate-limiting for tumorigenesis

ASNS is important for protection against apoptosis, activation of protein biosynthesis and induction of mTORC1 signaling. Consistent with a role for KRAS in driving expression of ASNS, increased ASNS protein was detected in lung tumors compared to normal adjacent tissue in a genetically engineered mouse model (Jackson et al., 2005) of KRAS-driven NSCLC (Figure 7A). To evaluate the role for ASNS in tumorigenesis in vivo, ASNS was over-expressed in two NSCLC xenograft models (Figure 7B, C, D, and S7A, B). Surprisingly, elevation of ASNS alone was sufficient to enhance tumor growth, indicating that the availability of asparagine for tumor growth is rate limiting. However, CRISPR-Cas9 mediated knockout of ASNS led to only moderate decrease in tumor growth in vivo (Figure 7E, F) likely due to uptake of asparagine from plasma. Depletion of plasma asparagine by

chemotherapeutic, L-asparaginase led to almost complete tumor stasis in tumors lacking ASNS (Figure 7E, F). This demonstrates that expression of ASNS mediates resistance to L-asparaginase in solid tumors (Hettmer et al., 2015), and suggests that modulation of KRAS-driven ASNS levels in combination with L-asparaginase treatment could be a therapeutic strategy in NSCLC.

The requirement of PI3K-AKT signaling for sustained expression of ASNS (Figure 3A, B), and the sensitization of tumors with ASNS loss to L-asparaginase suggested efficacy of a strategy combining AKT inhibition with L-asparaginase for treatment of NSCLC. To test the efficacy of this combinatorial therapy, xenograft tumors were treated with the AKT inhibitor MK-2206, L-asparaginase, or both. As single agent therapeutics, neither drug significantly suppressed tumor growth (Figure 7G, H). However, when combined, tumor growth was significantly decreased compared to either vehicle treated tumors or tumors treated with a single agent (Figure 7G, H). L-asparaginase treatment enhanced ASNS mRNA and protein levels, which were suppressed by AKT inhibition (Figure 7I, J). These results support a model whereby L-asparaginase treatment renders cells dependent on expression of ASNS, which requires transcriptional regulation by KRAS-AKT-NRF2, and translational regulation by phosphorylated eIF2 (Figure 8, left). However, when L-asparaginase treatment is combined with inhibition of AKT by MK2206, NRF2 and ATF4 levels are suppressed, impeding ASNS expression, and sensitizing cells to L-asparaginase therapy (Figure 8, right).

Overall, our studies identify KRAS-mediated ATF4 regulation as an important axis in amino acid homeostasis, and identify ASNS as an important target for metabolic regulation in KRAS-driven tumors. This work points to a previously unappreciated role for nutrient status in regulating the outcome of KRAS activation. Lastly, we demonstrate that inhibition of PI3K and depletion of extracellular asparagine represents a therapeutic strategy for treatment of NSCLC.

DISCUSSION

Tumor cells face a challenge in proliferating rapidly under conditions of limited nutrient availability while maintaining macromolecular precursors required for growth. While signaling downstream of KRAS has been widely studied, the role of this oncogene in helping tumor cells meet the challenge imposed by nutrient stress is not clear. Here we identify KRAS as a key regulator of the transcriptional response to nutrient deprivation and ATF4 as a key transcription factor regulated by KRAS in order to support amino acid homeostasis. Our results demonstrate that KRAS activates ATF4 and its target genes through a transcriptional mechanism mediated through PI3K and NRF2. Importantly we demonstrate that this pathway is required for full activation of ATF4. Furthermore, we identify expression of ASNS downstream of the KRAS-NRF2-ATF4 pathway as a key regulator of cancer cell proliferation. Lastly, we demonstrate that disruption of the KRAS-ATF4-ASNS pathway by AKT inhibition sensitizes NSCLC tumors to depletion of extracellular asparagine potentially establishing a new paradigm for combination therapy in NSCLC.

Identification of a KRAS-dependent glutamine response signature

Many groups have described gene expression alterations induced by KRAS in different cell types and model systems (Arena et al., 2007; Loboda et al., 2010; Sweet-Cordero et al., 2005), however, the importance of nutrient status in defining the transcriptional output of KRAS is not well defined. We demonstrate that KRAS plays a critical role in modulating the transcriptional response to nutrient stress. KRAS regulates a distinct set of genes under nutrient limited conditions, underscoring the importance of considering the nutritional status of a cell in order to evaluate the effect of oncogenic signaling. By considering nutrient stress as a variable, we uncovered KRAS-dependent regulation of the transcription factor ATF4. The clinical significance of this finding is underscored by the observation that genes suppressed by knockdown of KRAS in low glutamine correlate with poor clinical outcome.

Prior studies have suggested that KRAS increases utilization of glutamine for biosynthetic processes by enhancing flux of the TCA cycle intermediate oxaloacetate to aspartate (Gaglio et al., 2011). In pancreatic cancer, KRAS redirects the flux of glutamine to aspartate by up-regulating GOT1, resulting in enhanced NADPH production through the activity of malic enzyme (ME1) (Son et al., 2013). Aspartate also rescues S-phase arrest induced by nucleotide depletion in glutamine withdrawal in KRAS mutant cells (Patel et al., 2016). Here we demonstrate an additional role for aspartate as a substrate for asparagine biosynthesis, contributing to apoptotic suppression and tumorigenesis.

KRAS-PI3K-NRF2-ATF4 represents an important tumor metabolism axis

While PI3K is a canonical KRAS effector pathway (Schubbert et al., 2007), it remains unclear which substrates of the PI3K pathway are most critical for tumorigenesis. Furthermore, PI3K inhibitors alone are insufficient to treat KRAS-mutant NSCLC (Engelman et al., 2008). We demonstrate that during nutrient stress PI3K up-regulates NRF2 to support amino acid homeostasis through ATF4. NRF2 has been shown to modulate cellular metabolism through regulation of nucleotide biosynthesis, fatty acid synthesis, redox balance, and serine biosynthesis (Chartoumpekis et al., 2015; DeNicola et al., 2015). However, the importance of NRF2-mediated regulation of ATF4 in global amino acid homeostasis has not been appreciated. Our studies demonstrate that in addition to serine biosynthesis, the NRF2-ATF4 axis plays a role in uptake of most amino acids, and asparagine biosynthesis. This furthers the model of NRF2 as a master metabolic regulator.

PI3K is specifically important for cell survival downstream of oncogenic KRAS (Castellano et al., 2013). However, depending on the genetic context, and nutrient conditions, KRAS signaling through PI3K can promote apoptosis. Cells bearing mutations in both KRAS and KEAP1 are exquisitely sensitive to apoptosis upon amino acid deprivation, which is dependent on PI3K-mediated enhancement of ATF4 activity. This demonstrates a genotype specific vulnerability, and indicates that cancer patients with these mutations may benefit therapeutically from amino acid transporter inhibition.

Amino acid homeostasis by KRAS-ATF4 in tumorigenesis

While ATF4 can be either oncogenic or tumor suppressive, our results indicate that while ATF4 can drive both proliferation and apoptosis in NSCLC in vivo, loss of ATF4 suppresses

tumor growth. Through ATF4, KRAS regulates expression of many vital amino acid transporters, and is required to maintain intracellular amino acid levels. Amino acids provide most of the biomass for growing cells despite the high levels of consumption of glucose and glutamine (Hosios et al., 2016), indicating that KRAS-mediated regulation of amino acid transporters is crucial for tumor growth. While KRAS has been shown to regulate macropinocytosis for amino acid uptake in pancreatic cancer (Commisso et al., 2013), more recent data suggest tissue-specific dependencies and indicate greater use of amino acid transport rather than macropinocytosis in NSCLC compared to pancreatic cancer (Mayers et al., 2016). This work highlighted several genes key to the ability of NSCLC to utilize amino acids from plasma including Slc7a5 (LAT1), which we show here to be regulated by KRAS and by ATF4, as well as BCAT1 and BCAT2, which are also ATF4 targets. Taken together these results suggest that KRAS-mediated regulation of ATF4 is of particular importance for NSCLC amino acid metabolism.

Suppression of ASNS by AKT inhibition sensitizes cancer cells to L-asparaginase, suggesting a therapeutic opportunity in NSCLC

Our study and others have found that intracellular levels of asparagine are low compared with other amino acids (Zhang et al., 2014). While these levels are sufficient to support tumor cell proliferation, it allows asparagine to act as a sensitive gauge of nutrient availability. ASNS overexpression allows enhanced tumor growth, suggesting that asparagine is a rate-limiting nutrient for cancer. The use of asparagine depletion as a cancer therapeutic is well established in acute lymphocytic leukemias (ALL). Most ALL cells lack ASNS and are dependent on plasma asparagine, thus depletion of extracellular asparagine by L-asparaginase leads to cell death (Batool et al., 2016). L-asparaginase-resistant leukemia cells are sensitive to apoptosis by inhibition of ASNS, indicating that ASNS up-regulation is the key mechanism of resistance to this drug (Ikeuchi et al., 2012). It has long been known that solid tumors express ASNS and are resistant to the effect of depletion of extracellular pools of asparagine by L-asparaginase (Balasubramanian et al., 2013). We and others have shown that ASNS is required for resistance to L-asparaginase (Lorenzi et al., 2006). Because we have uncovered the PI3K-AKT dependent regulation of ASNS downstream of ATF4, we were able to demonstrate that pharmacological inhibition of this pathway sensitizes NSCLC tumors to L-asparaginase therapy. This represents a potential treatment approach for KRAS-driven NSCLC patients.

STAR METHODS

CONTACT FOR REAGENT AND RESOURCE SHARING

Further information and requests for resources and reagents should be directed to and will be fulfilled by the Lead Contact, E. Alejandro Sweet-Cordero (Alejandro.Sweet-Cordero@ucsf.edu).

EXPERIMENTAL MODEL AND SUBJECT DETAILS

Cell lines—All cell lines were obtained from ATCC: NCI-H460, A549, NCI-H2009, NCI-H358, NCI-H1792, NCI-H23, NCI-H2122, NCI-H1944, NCI-H1437, NCI-H1568, NCI-H522, NCI-H1650, NCI-H441, NCI-H2347 and maintained in RPMI supplemented with

10% bovine growth serum (BGS), 4mM glutamine, and penicillin and streptomycin (P/S). Experiments were performed in DMEM supplemented with 10% BGS, indicated glutamine concentration, and P/S. Cells were incubated at 37°C in 5% CO_2. Cells were routinely tested to exclude Mycoplasma contamination. Comparison of STR testing (Promega GenPrint10) on genomic DNA from our cell lines to ATCC data confirmed the identity of the cell lines.

Mice

KrasG12D;Trp53 mice: Lox-stop-lox-Kras^{G12D} (Jackson et al., 2001); Trp53$^{fl/fl}$ (Jonkers et al., 2001) mice were maintained in a viral-free environment. Adenoviral-Cre (University of Iowa) was delivered intranasally to mice between 10–14 weeks of age. Tumor-bearing mice were sacrificed approximately 12 weeks after infection (~24 weeks of age). All animal experiments were approved by the Stanford University School of Medicine Committee on Amino Care (APLAC). Equal number of male and female mice were utilized.

NSG mice: NOD scid IL2Rg^{null} (NSG) mice were obtained from Jackson Laboratory, Bar Harbor, Maine, USA, and bred in the barrier facility at Stanford University. Both male and female mice were used for xenograft studies. Xenograft tumors were injected when mice were approximately 8–10 weeks of age.

Human lung cancer data—Normalized gene expression (RSEM Level 3 v.2) for the TCGA Lung Adenocarcinoma (LUAD) cohort consisting of 585 RNA-Seq samples were downloaded from the Broad Institute data portal site (GDAC Firehose, url: https://gdac.broadinstitute.org/). Details and specific download links with hash key are listed in the Key Resources Table. Somatic mutations for the same cohort were downloaded from the Xena Functional Genomics Explorer website (https://xenabrowser.net/).

METHOD DETAILS

Generation of cell lines expressing shRNA, or over-expressing AKT or ASNS —Filtered lentiviral supernatant from HEK293T cells transfected with pLKO.1-Tet shGFP or shKRAS was added to NSCLC cell lines (A549, H460, H2009 or H358) with polybrene (8μg/mL). After 72-hour incubation, cells were selected in puromycin (2μg/mL) for 72 hours. Stable knockdown of ATF4, NRF2, and ASNS were achieved as described above, but with pLKO.1. AKT and ASNS overexpression were achieved by infection of NSCLC cell lines with retroviruses produced with pCL-Ampho transfection. Cells were then selected for 72 hours in neomycin/G418 (2.5mg/mL) or blasticidin (10μg/mL), respectively. AZD6244, BKM120, MK2206, Rapamycin, or BRD7389 were added to cells 60 hours, with last 36 hrs in glutamine-free DMEM.

Generation of ASNS or ATF4 knock-out cell lines—Filtered lentiviral supernatant from HEK293T cells transfected with MCB306 sgGFP, sgASNS, or sgATF4 and lentiCas9 was added to H460 cells with polybrene (8μg/mL). After 72-hr incubation, cells were selected in puromycin (2μg/mL) for 72 hours. Cells were then plated at low density for a period or 1–2 weeks. Clones were picked and expanded. Confirmation of loss of ATF4 or ASNS was confirmed by Western blotting. See Supplemental Table S4 for sgRNA sequences.

Glutamine deprivation studies—Cells were switched from complete RPMI medium to DMEM containing 10% BGS, penicillin and streptomycin, along with indicated concentration of glutamine. Cells were maintained at 37°C for indicated time periods at 5% CO_2.

Plasmids and cloning—KRAS targeting hairpins were cloned into pLKO.1-Tet as per the User Manual. ASNS and ATF4 sgRNAs were cloned into MCB306 vector. Cas9 expression was achieved with lentiCas9. ASNS cDNA was purchased from the ASU DNA repository (DNASU) as pDONR221-ASNS. LR Clonase was used to clone ASNS from pDONR221 into the retroviral vector pQXCI-Blast. pLNCX-HA-Akt vectors were obtained by AddGene. Lentiviral and retroviral vectors were transduced into the indicated cells using standard protocols. See Supplemental Table S4 for shRNA and sgRNA sequences.

Western blotting—Cells were washed in ice cold PBS, then lysed in Triton buffer (20mM Tris (pH7.5), 150mM NaCl, 1mM EDTA, 1% Triton X-100, 10mM NaF, 2.5mM sodium pyrophosphate, 1mM β-glycerophosphate, 1mM Na_3VO_4 supplemented with protease inhibitors (Roche). Cleared supernatants were subjected to protein quantification by BCA kit (Pierce). Proteins were resolved by SDS-PAGE, transferred to PVDF membranes, and blocked in 5% non-fat dry milk. Primary antibodies were incubated overnight at 4°C. Where necessary, quantification was performed using ImageJ software. Information on antibodies used is found in the Key Resources Table.

Intracellular amino acid analysis—Briefly, amino acids were analyzed as underivatized compounds by liquid chromatography tandem mass spectrometry (LC-MS/MS) using an Agilent 6460 tandem mass spectrometer. Cells were trypsinized, washed in PBS and incubated in 50μL 6% sulfosalysilic acid (1:1) to deproteinize. Samples were spun for 5 minutes at 13,000rpm, and supernatants were diluted with 2μM tridecafluoroheptanoic acid (TDFHA) containing 0.375μM glucosaminic acid and 0.25μM *S*-2-aminoethylcysteine as internal standards. Chromatographic separation was achieved using a porous graphitic carbon (PGC) column (Thermo Fisher Scientific), in series with a fused-core column (Advanced Materials Technology), using a gradient of increasing acetonitrile concentration in TDFHA. Amino acids were analyzed in the positive ion mode and detected by scheduled selective reaction monitoring (SRM). Data were acquired using MassHunter Workstation Acquisition version B.02.01, and exported to Excel (2007edition, Microsoft Corporation) for further calculations. Quantitative values were obtained by relating chromatographic peak areas to those derived from externally run calibration standards. Further details in (Le et al., 2014).

Amino acid uptake assays—Cells grown for 72 hours in indicated conditions were plated in 6-well plates. Growth medium was with glutamine-free DMEM containing 2μCi ^{3}H-Gln or ^{3}H-Leu for 15 minutes. Cells were washed 3× with ice-cold PBS, lysed with 500μL 0.2% SDS/0.2N NaOH, and incubated for 1 hour at room temperature. 50μL 1N HCl was added to neutralize the lysates, then added to scintillation fluid (EcoLume). Scintillation counts were measured on a LS6500 Beckman Coulter and normalized to cell number.

Leucine incorporation assay—Cells grown for 48 hours in indicated conditions were plated in 6-well plates. 24 hours later, 2μCi ^{3}H-leucine was added for 5, 15 or 30 minutes. Cells were washed 3× with ice cold PBS, lysed in 500μL ice cold 10% perchloric acid, and incubated for 20 minutes. Cells were scraped into microfuge tubes, and spun for 10 minutes at 15,000*xg*. Supernatant was discarded, and pellets were washed with 500μL 10% perchloric acid then spun for 10 minutes at 15,000*x*g. Supernatant was discarded, and pellets were resuspended in 0.2N NaOH to solubilize. Sample was added to scintillation fluid (EcoLume), and counts were measured and normalized to cell number.

Methionine uptake and incorporation—Cells were grown for 48 hours in indicated conditions, and plated to 6-well plates. After 24 hours, cells were pulsed with 5μCi ^{35}S-methionine for 30, 60 or 120 minutes. At indicated times, cells were quickly washed with ice cold PBS supplemented with 50μg/mL of cycloheximide, and then lysed in 1% Triton-X Buffer (see Western blotting) and scraped to microfuge tubes. For analyses, cell lysates were prepared using standard procedures followed by protein quantification (Bradford). Equal amounts of total protein were monitored for methionine/cysteine uptake and incorporation. Uptake was monitored by scintillation counting and incorporation by separating proteins on a 10% SDS polyacrylamide gel followed by transfer to PVDF membrane. Membranes were exposed to autoradiography film for 6 days and then developed. ^{35}S methionine/cysteine incorporation was quantified using ImageJ software to analyze optical density and normalized to β-actin levels probed on same membrane. Results are presented as intensity of S^{35} bands compared to intensity of actin bands.

Cell proliferation and viability assay—Cells were seeded in 96 well plates (1000 cells/well) in indicated conditions. 3-[4,5-dimethylthiazol-2-yl]-2,5-diphenyl tetrazolium bromide (MTT) was added for 4 hrs followed by lysis with 10% SDS in 0.01M HCl). Absorbance at 540nm was read on indicated days on a Synergy H1 hybrid plate reader (BioTek). All data was compared to first reading.

RT-qPCR analysis—RNA was isolated using TRIZOL reagent (Invitrogen) following manufacturer's specifications. cDNA was synthesized with a Maxima kit (Thermo Scientific). RT-PCR was performed using SYBR Green (Applied Biosystems). See Supplemental Table S4 for RT-qPCR primer sequences.

Xenograft tumor studies—1×10^{6} cells were injected subcutaneously into the 2 lower flanks of NOD scid gamma (NSG) mice. L-asparaginase (3UI/kg) was administered daily for 2 weeks via IP injection once xenograft tumors reached a size of 200 mm^3 (3 weeks). MK2206 (120mg/kg in 20% Captisol) was given by oral gavage 3 times per week for 2 weeks.

Cell cycle analysis—Cells were trypsinized, then 1×10^{6} cells were washed 3 times in cold PBS. In the third wash, cells were fixed by adding ice-cold 100% ethanol drop-wise with gentle vortexing until a 70% ethanol solution is achieved. After overnight fixation (cells can be stored for several weeks in 70% EtOH), cells were washed three times with 1mL PBS, then incubated for 1 hour at room temperature in final wash with 50μL of 100μg/mL RNase. 200μL of 50μg/mL propidium iodide was added. Cells were analyzed for PI by flow

cytometry on a Fortessa Cell Analyzer (BD Biosciences). FlowJo software was used to perform cell-cycle analysis.

Chromatin immunoprecipitation—Cells cultured as indicated were cross-linked in 1% formaldehyde with gentle rocking at room temperature for 10 minutes. Cross-linking was arrested by addition of 0.125M glycine with gentle rocking for 5 minutes at room temperature. Cross-linked cells were scraped into 50 mL conicals and washed twice with PBS. Cross-linked cells were resuspended in Swelling Solution (0.1M Tris pH 7.6, 10mM KOAc, 15mM MgOAc, 1% NP40, 1mM PMSF, and protease inhibitors), and incubated on ice for 20 minutes with occasional flicking to stir. Cells were dounced using a 2mL B-dounce for 15 strokes. Nuclei were pelleted by centrifugation at 2500xg for 5 minutes at 4°C. Supernatant was discarded, and nuclei were resuspended in Nuclei Lysis Solution (50mM Tris-Cl pH 8.0, 10mM EDTA, 1% SDS, 1mM PMSF, and protease inhibitors), and incubated on ice for 10 minutes. Chromatin was sheared to an average fragment size of 500bp using a Covaris S2 Ultrasonicator, duty cycle 5, intensity 4, cycles/burst 200, time 60 secs for 14 cycles (Covaris, Woburn, MA). Sheared chromatin was diluted in IP Diluted Buffer, and divided into aliquots for immunoprecipitation. anti-ATF4 antibody (#11815, Cell Signaling) or Normal Rabbit IgG control (#2729, Cell Signaling) were added to chromatin samples, followed by overnight incubation at 4ºC, with rotation. Antibody-chromatin complexes were captured with Protein G Dynabeads (Life Technologies) at 4 ºC for 4 h, with rotation. Beads were washed 2× with Dialysis buffer, 3× with IP wash buffer, and resuspended in IP elution buffer. Supernatant containing eluted chromatin was removed from the beads and the cross links were reversed by incubating samples overnight at 67 ºC, and purified using a QIAquick PCR purification kit (Qiagen). Real-time quantitative PCR was performed by using Applied Biosystems 7900HT system and detected with Perfecta SYBR Green SuperMix (Quanta BioSciences). See Supplemental Table S4 for RT-qPCR primer sequences.

ChIP buffer compositions: Swelling Buffer (0.1M Tris pH 7.6, 10mM KOAc, 15mM MgOAc, 1% NP40, 1mM PMSF, and protease inhibitors). Lysis Buffer (50mM Tris-Cl pH 8.0, 10mM EDTA, 1% SDS, 1mM PMSF, and protease inhibitors). IP Dilution Buffer (0.01% SDS, 1.1% Triton X100, 1.2mM EDTA, 16.7mM Tris-Cl pH 8.0, 167 mM NaCl, 1mM PMSF, and protease inhibitors). Dialysis Buffer (2mM EDTA, and 50mM Tris-Cl pH 8.0). IP Wash Buffer (100mM Tris-Cl pH 8.0, 500mM LiCl, 1% aka NP40, 1% Deoxycholic Acid, 1mM PMSF, and protease inhibitors). IP Elution Buffer (50mM $NaHCO_3$, 1% SDS).

Gene Expression analysis—RNA was isolated using TRIZOL followed by passage over an RNeasy column (QIAGEN). RNA was prepared for hybridization to human genome Illumina HumanHT-12v4.0 platform according to the manufacturer's instructions (Illumina) by the Stanford Functional Genomics Core. Unless specified, all analysis were carried out using R. Software databases and versions used are listed in Supplemental Table S3 (R-markdown file) under session info. Microarrays for three experiments were generated. Each experiment consists of four cell lines with the following conditions: 1) Low Glutamine (Q) vs. High Q, 2) shGFP vs. shKRAS in low Q, 3) shGFP and shKRAS in high Q (N=4 per condition). Raw probe intensities were background corrected, log2 transformed and quantile

normalized using the lumi package. Normalized data were checked for quality and determined to be free of outliers by analysis using box plots, density plots and MA plots. Differential expression and fold changes were calculated separately for each of the three comparisons using a linear model provided by the the limma package. Genes were considered differentially expressed if p-value < 0.05 and 1.4 < Fold Change (FC) < −1.4. TCGA lung adenocarcinoma datasets and clinical data for survival analysis were collected from Broad Institute (version stddata_2016_01_28). TCGA lung adenocarcinoma (LUAD) somatic mutation data were downloaded from UCSC Xena (version 2015-11-14). Overall survival curves were analyzed using the Kaplan Meir method and p-value were calculated using the log-rank (Mantel-Haenszel) test. Cox proportional hazards and associated p-value were calculated while controlling for age. Gene signatures for survival analysis were calculated as described in Supplemental Table S3. We selected gene cycle genes by importing the differentially expressed genes into PANTHER ontology and filtering out genes under the GO term “cell-cycle” (GO:0007049). Ingenuity Pathway Analysis was used for network and pathway analysis. Datasets were imported and a core analysis feature was used to compare both canonical and upstream analysis between three different experiments. Upstream transcription analysis was conducted using Biobase and accompanying TRANSFAC database (Release 2016.1) using the default −500 − +100 bp upstream of the transcription start site of each gene. All microarray datasets were deposited to the GEO repository, accession series, GSE81644 or subseries, GSE81641, GSE81642, GSE81643.

QUANTIFICATION AND STATISTICAL ANALYSIS

The specific statistical tests used are indicated in the figure legends and were calculated using GraphPad Prism. Unpaired Student’s t-test was used to compare two groups. Details for analysis are included in figure legends.

DATA AND SOFTWARE AVAILABILITY

The microarray data reported in this paper has been deposited to NCBI GEO under accession number GSE81644. Human lung cancer gene expression data utilized in this paper can be accessed at the TCGA network (http://cancergenome.nih.gov/).

Supplementary Material

Refer to Web version on PubMed Central for supplementary material.

Acknowledgments

D.M.G. was funded by an American Cancer Society Post-doctoral Fellowship (PF-12-189-01). E.A.S.C. was funded by PHS Grant 4R01CA129562 (National Cancer Institute). D.R.S. was funded by PHS Grant CA09302, (National Cancer Institute). We thank Julien Sage, Peter Jackson, Michael Bassik, Steve Artandi, Laura Attardi and Monte Winslow for helpful suggestions.

References

Afonyushkin T, Oskolkova OV, Philippova M, Resink TJ, Erne P, Binder BR, Bochkov VN. Oxidized phospholipids regulate expression of ATF4 and VEGF in endothelial cells via NRF2-dependent mechanism: novel point of convergence between electrophilic and unfolded protein stress pathways. Arterioscler Thromb Vasc Biol. 2010; 30:1007–1013. [PubMed: 20185790]

Ameri K, Harris AL. Activating transcription factor 4. Int J Biochem Cell Biol. 2008; 40:14–21. [PubMed: 17466566]

Arena S, Isella C, Martini M, de Marco A, Medico E, Bardelli A. Knock-in of oncogenic Kras does not transform mouse somatic cells but triggers a transcriptional response that classifies human cancers. Cancer Res. 2007; 67:8468–8476. [PubMed: 17875685]

Arnstein HR, Barwick CW, Lange JD, Thomas HD. Control of protein synthesis by amino acid supply. The effect of asparagine deprivation on the translation of messenger RNA in reticulocyte lysates. FEBS letters. 1986; 194:146–150. [PubMed: 3940884]

Balasubramanian MN, Butterworth EA, Kilberg MS. Asparagine synthetase: regulation by cell stress and involvement in tumor biology. American journal of physiology Endocrinology and metabolism. 2013; 304:E789–799. [PubMed: 23403946]

Batool T, Makky EA, Jalal M, Yusoff MM. A Comprehensive Review on LAsparaginase and Its Applications. Applied biochemistry and biotechnology. 2016; 178:900–923. [PubMed: 26547852]

Bryant KL, Mancias JD, Kimmelman AC, Der CJ. KRAS: feeding pancreatic cancer proliferation. Trends in biochemical sciences. 2014; 39:91–100. [PubMed: 24388967]

Campeau E, Ruhl VE, Rodier F, Smith CL, Rahmberg BL, Fuss JO, Campisi J, Yaswen P, Cooper PK, Kaufman PD. A versatile viral system for expression and depletion of proteins in mammalian cells. PLoS One. 2009; 4:e6529. [PubMed: 19657394]

Castellano E, Sheridan C, Thin MZ, Nye E, Spencer-Dene B, Diefenbacher ME, Moore C, Kumar MS, Murillo MM, Gronroos E, et al. Requirement for interaction of PI3-kinase p110alpha with RAS in lung tumor maintenance. Cancer Cell. 2013; 24:617–630. [PubMed: 24229709]

Castilho BA, Shanmugam R, Silva RC, Ramesh R, Himme BM, Sattlegger E. Keeping the eIF2 alpha kinase Gcn2 in check. Biochim Biophys Acta. 2014; 1843:1948–1968. [PubMed: 24732012]

Chartoumpekis DV, Wakabayashi N, Kensler TW. Keap1/Nrf2 pathway in the frontiers of cancer and non-cancer cell metabolism. Biochemical Society transactions. 2015; 43:639–644. [PubMed: 26551705]

Commisso C, Davidson SM, Soydaner-Azeloglu RG, Parker SJ, Kamphorst JJ, Hackett S, Grabocka E, Nofal M, Drebin JA, Thompson CB, et al. Macropinocytosis of protein is an amino acid supply route in Ras-transformed cells. Nature. 2013; 497:633–637. [PubMed: 23665962]

DeBerardinis RJ, Lum JJ, Hatzivassiliou G, Thompson CB. The biology of cancer: metabolic reprogramming fuels cell growth and proliferation. Cell Metab. 2008; 7:11–20. [PubMed: 18177721]

DeNicola GM, Chen PH, Mullarky E, Sudderth JA, Hu Z, Wu D, Tang H, Xie Y, Asara JM, Huffman KE, et al. NRF2 regulates serine biosynthesis in non-small cell lung cancer. Nat Genet. 2015; 47:1475–1481. [PubMed: 26482881]

DeNicola GM, Karreth FA, Humpton TJ, Gopinathan A, Wei C, Frese K, Mangal D, Yu KH, Yeo CJ, Calhoun ES, et al. Oncogene-induced Nrf2 transcription promotes ROS detoxification and tumorigenesis. Nature. 2011; 475:106–109. [PubMed: 21734707]

Dey S, Sayers CM, Verginadis II, Lehman SL, Cheng Y, Cerniglia GJ, Tuttle SW, Feldman MD, Zhang PJ, Fuchs SY, et al. ATF4-dependent induction of heme oxygenase 1 prevents anoikis and promotes metastasis. J Clin Invest. 2015; 125:2592–2608. [PubMed: 26011642]

Donnelly N, Gorman AM, Gupta S, Samali A. The eIF2alpha kinases: their structures and functions. Cellular and molecular life sciences : CMLS. 2013; 70:3493–3511. [PubMed: 23354059]

Engelman JA, Chen L, Tan X, Crosby K, Guimaraes AR, Upadhyay R, Maira M, McNamara K, Perera SA, Song Y, et al. Effective use of PI3K and MEK inhibitors to treat mutant Kras G12D and PIK3CA H1047R murine lung cancers. Nat Med. 2008; 14:1351–1356. [PubMed: 19029981]

Gaglio D, Metallo CM, Gameiro PA, Hiller K, Danna LS, Balestrieri C, Alberghina L, Stephanopoulos G, Chiaradonna F. Oncogenic K-Ras decouples glucose and glutamine metabolism to support cancer cell growth. Molecular systems biology. 2011; 7:523. [PubMed: 21847114]

Gorrini C, Harris IS, Mak TW. Modulation of oxidative stress as an anticancer strategy. Nature reviews Drug discovery. 2013; 12:931–947. [PubMed: 24287781]

Han J, Back SH, Hur J, Lin YH, Gildersleeve R, Shan J, Yuan CL, Krokowski D, Wang S, Hatzoglou M, et al. ER-stress-induced transcriptional regulation increases protein synthesis leading to cell death. Nat Cell Biol. 2013; 15:481–490. [PubMed: 23624402]

Han K, Jeng EE, Hess GT, Morgens DW, Li A, Bassik MC. Synergistic drug combinations for cancer identified in a CRISPR screen for pairwise genetic interactions. Nat Biotechnol. 2017; 35:463–474. [PubMed: 28319085]

Hao Y, Samuels Y, Li Q, Krokowski D, Guan BJ, Wang C, Jin Z, Dong B, Cao B, Feng X, et al. Oncogenic PIK3CA mutations reprogram glutamine metabolism in colorectal cancer. Nature communications. 2016; 7:11971.

Harding HP, Zhang Y, Zeng H, Novoa I, Lu PD, Calfon M, Sadri N, Yun C, Popko B, Paules R, et al. An integrated stress response regulates amino acid metabolism and resistance to oxidative stress. Molecular cell. 2003; 11:619–633. [PubMed: 12667446]

He CH, Gong P, Hu B, Stewart D, Choi ME, Choi AM, Alam J. Identification of activating transcription factor 4 (ATF4) as an Nrf2-interacting protein. Implication for heme oxygenase- 1 gene regulation. J Biol Chem. 2001; 276:20858–20865. [PubMed: 11274184]

Hensley CT, Wasti AT, DeBerardinis RJ. Glutamine and cancer: cell biology, physiology, and clinical opportunities. The Journal of clinical investigation. 2013; 123:3678–3684. [PubMed: 23999442]

Hettmer S, Schinzel AC, Tchessalova D, Schneider M, Parker CL, Bronson RT, Richards NG, Hahn WC, Wagers AJ. Functional genomic screening reveals asparagine dependence as a metabolic vulnerability in sarcoma. Elife. 2015:4.

Hetz C. The unfolded protein response: controlling cell fate decisions under ER stress and beyond. Nature reviews Molecular cell biology. 2012; 13:89–102. [PubMed: 22251901]

Hosios AM, Hecht VC, Danai LV, Johnson MO, Rathmell JC, Steinhauser ML, Manalis SR, Vander Heiden MG. Amino Acids Rather than Glucose Account for the Majority of Cell Mass in Proliferating Mammalian Cells. Developmental cell. 2016; 36:540–549. [PubMed: 26954548]

Hyde R, Taylor PM, Hundal HS. Amino acid transporters: roles in amino acid sensing and signalling in animal cells. The Biochemical journal. 2003; 373:1–18. [PubMed: 12879880]

Ikeuchi H, Ahn YM, Otokawa T, Watanabe B, Hegazy L, Hiratake J, Richards NG. A sulfoximine-based inhibitor of human asparagine synthetase kills L-asparaginase-resistant leukemia cells. Bioorganic & medicinal chemistry. 2012; 20:5915–5927. [PubMed: 22951255]

Jackson EL, Olive KP, Tuveson DA, Bronson R, Crowley D, Brown M, Jacks T. The differential effects of mutant p53 alleles on advanced murine lung cancer. Cancer research. 2005; 65:10280–10288. [PubMed: 16288016]

Jackson EL, Willis N, Mercer K, Bronson RT, Crowley D, Montoya R, Jacks T, Tuveson DA. Analysis of lung tumor initiation and progression using conditional expression of oncogenic K-ras. Genes Dev. 2001; 15:3243–3248. [PubMed: 11751630]

Jain AK, Jaiswal AK. GSK-3beta acts upstream of Fyn kinase in regulation of nuclear export and degradation of NF-E2 related factor 2. J Biol Chem. 2007; 282:16502–16510. [PubMed: 17403689]

Jonkers J, Meuwissen R, van der Gulden H, Peterse H, van der Valk M, Berns A. Synergistic tumor suppressor activity of BRCA2 and p53 in a conditional mouse model for breast cancer. Nat Genet. 2001; 29:418–425. [PubMed: 11694875]

Krall AS, Xu S, Graeber TG, Braas D, Christofk HR. Asparagine promotes cancer cell proliferation through use as an amino acid exchange factor. Nat Commun. 2016; 7:11457. [PubMed: 27126896]

Le A, Ng A, Kwan T, Cusmano-Ozog K, Cowan TM. A rapid, sensitive method for quantitative analysis of underivatized amino acids by liquid chromatography-tandem mass spectrometry (LC-MS/MS). Journal of chromatography B, Analytical technologies in the biomedical and life sciences. 2014; 944:166–174. [PubMed: 24316529]

Levine AJ, Puzio-Kuter AM. The control of the metabolic switch in cancers by oncogenes and tumor suppressor genes. Science. 2010; 330:1340–1344. [PubMed: 21127244]

Loboda A, Nebozhyn M, Klinghoffer R, Frazier J, Chastain M, Arthur W, Roberts B, Zhang T, Chenard M, Haines B, et al. A gene expression signature of RAS pathway dependence predicts response to PI3K and RAS pathway inhibitors and expands the population of RAS pathway activated tumors. BMC Med Genomics. 2010; 3:26. [PubMed: 20591134]

Lorenzi PL, Reinhold WC, Rudelius M, Gunsior M, Shankavaram U, Bussey KJ, Scherf U, Eichler GS, Martin SE, Chin K, et al. Asparagine synthetase as a causal, predictive biomarker for L-

asparaginase activity in ovarian cancer cells. Mol Cancer Ther. 2006; 5:2613–2623. [PubMed: 17088436]

Mayers JR, Torrence ME, Danai LV, Papagiannakopoulos T, Davidson SM, Bauer MR, Lau AN, Ji BW, Dixit PD, Hosios AM, et al. Tissue of origin dictates branched-chain amino acid metabolism in mutant Kras-driven cancers. Science. 2016; 353:1161–1165. [PubMed: 27609895]

Miyamoto N, Izumi H, Miyamoto R, Bin H, Kondo H, Tawara A, Sasaguri Y, Kohno K. Transcriptional regulation of activating transcription factor 4 under oxidative stress in retinal pigment epithelial ARPE-19/HPV-16 cells. Investigative ophthalmology & visual science. 2011; 52:1226–1234. [PubMed: 21087962]

Patel D, Menon D, Bernfeld E, Mroz V, Kalan S, Loayza D, Foster DA. Aspartate Rescues S-phase Arrest Caused by Suppression of Glutamine Utilization in KRas-driven Cancer Cells. J Biol Chem. 2016; 291:9322–9329. [PubMed: 26921316]

Qing G, Li B, Vu A, Skuli N, Walton ZE, Liu X, Mayes PA, Wise DR, Thompson CB, Maris JM, et al. ATF4 regulates MYC-mediated neuroblastoma cell death upon glutamine deprivation. Cancer Cell. 2012; 22:631–644. [PubMed: 23153536]

Ramaswamy S, Nakamura N, Vazquez F, Batt DB, Perera S, Roberts TM, Sellers WR. Regulation of G1 progression by the PTEN tumor suppressor protein is linked to inhibition of the phosphatidylinositol 3-kinase/Akt pathway. Proc Natl Acad Sci U S A. 1999; 96:2110–2115. [PubMed: 10051603]

Sanjana NE, Shalem O, Zhang F. Improved vectors and genome-wide libraries for CRISPR screening. Nat Methods. 2014; 11:783–784. [PubMed: 25075903]

Schubbert S, Bollag G, Shannon K. Deregulated Ras signaling in developmental disorders: new tricks for an old dog. Current opinion in genetics & development. 2007; 17:15–22. [PubMed: 17208427]

Son J, Lyssiotis CA, Ying H, Wang X, Hua S, Ligorio M, Perera RM, Ferrone CR, Mullarky E, Shyh-Chang N, et al. Glutamine supports pancreatic cancer growth through a KRAS-regulated metabolic pathway. Nature. 2013; 496:101–105. [PubMed: 23535601]

Sweet-Cordero A, Mukherjee S, Subramanian A, You H, Roix JJ, Ladd-Acosta C, Mesirov J, Golub TR, Jacks T. An oncogenic KRAS2 expression signature identified by cross-species gene-expression analysis. Nat Genet. 2005; 37:48–55. [PubMed: 15608639]

TCGA. Comprehensive molecular profiling of lung adenocarcinoma. Nature. 2014; 511:543–550. [PubMed: 25079552]

Vander Heiden MG, Cantley LC, Thompson CB. Understanding the Warburg effect: the metabolic requirements of cell proliferation. Science. 2008; 324:1029–1033.

Vattem KM, Wek RC. Reinitiation involving upstream ORFs regulates ATF4 mRNA translation in mammalian cells. Proceedings of the National Academy of Sciences of the United States of America. 2004; 101:11269–11274. [PubMed: 15277680]

Wang S, Chen XA, Hu J, Jiang JK, Li Y, Chan-Salis KY, Gu Y, Chen G, Thomas C, Pugh BF, Wang Y. ATF4 Gene Network Mediates Cellular Response to the Anticancer PAD Inhibitor YW3–56 in Triple-Negative Breast Cancer Cells. Mol Cancer Ther. 2015; 14:877–888. [PubMed: 25612620]

Wiederschain D, Wee S, Chen L, Loo A, Yang G, Huang A, Chen Y, Caponigro G, Yao YM, Lengauer C, et al. Single-vector inducible lentiviral RNAi system for oncology target validation. Cell Cycle. 2009; 8:498–504. [PubMed: 19177017]

Ye J, Kumanova M, Hart LS, Sloane K, Zhang H, De Panis DN, Bobrovnikova-Marjon E, Diehl JA, Ron D, Koumenis C. The GCN2-ATF4 pathway is critical for tumour cell survival and proliferation in response to nutrient deprivation. EMBO J. 2010; 29:2082–2096. [PubMed: 20473272]

Ye J, Mancuso A, Tong X, Ward PS, Fan J, Rabinowitz JD, Thompson CB. Pyruvate kinase M2 promotes de novo serine synthesis to sustain mTORC1 activity and cell proliferation. Proceedings of the National Academy of Sciences of the United States of America. 2012; 109:6904–6909. [PubMed: 22509023]

Ye P, Mimura J, Okada T, Sato H, Liu T, Maruyama A, Ohyama C, Itoh K. Nrf2- and ATF4-dependent upregulation of xCT modulates the sensitivity of T24 bladder carcinoma cells to proteasome inhibition. Molecular and cellular biology. 2014; 34:3421–3434. [PubMed: 25002527]

Zhang J, Fan J, Venneti S, Cross JR, Takagi T, Bhinder B, Djaballah H, Kanai M, Cheng EH, Judkins AR, et al. Asparagine plays a critical role in regulating cellular adaptation to glutamine depletion. Mol Cell. 2014; 56:205–218. [PubMed: 25242145]

Zoncu R, Efeyan A, Sabatini DM. mTOR: from growth signal integration to cancer, diabetes and ageing. Nature reviews Molecular cell biology. 2011; 12:21–35. [PubMed: 21157483]

Significance

KRAS is mutated in approximately 30% of non-small cell lung cancer patients, yet no therapeutic strategy to target it has proven successful. Many studies defining the role for KRAS in driving tumorigenesis fail to account for potential stress conditions experienced physiologically. Nutrient deprivation reveals a role for KRAS in supporting amino acid transport and metabolism, and uncovers a therapeutic vulnerability in asparagine biosynthesis. In addition, our studies identify the coordinate mutation of KRAS and KEAP1 as a key determinant of the outcome of nutrient stress.

Highlights

- KRAS regulates the transcriptional response to nutrient stress via ATF4.
- The PI3K-AKT pathway modulates NRF2 activity to regulate ATF4.
- ASNS is a key target of the KRAS-ATF4 axis in NSCLC.
- AKT inhibition with L-asparaginase treatment is an effect combination therapy.

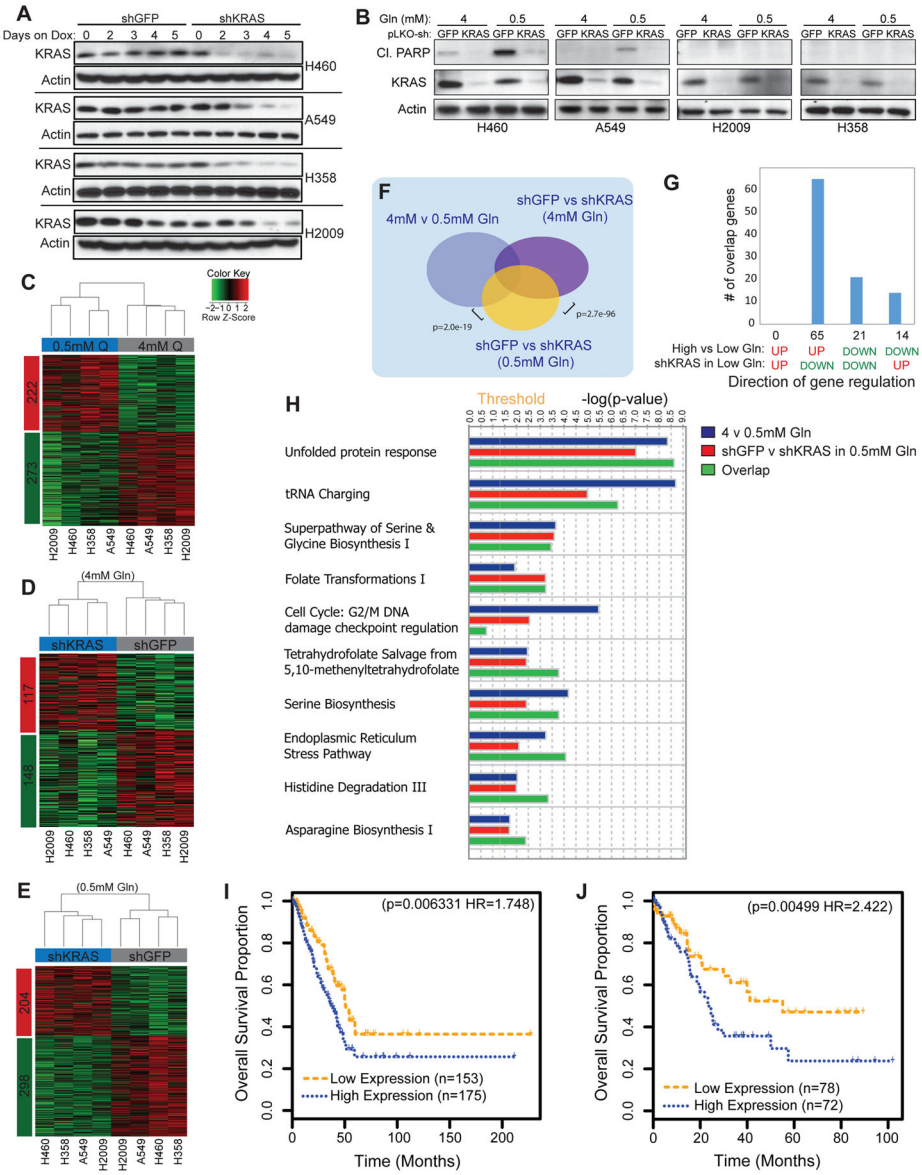

Figure 1. Response to KRAS knockdown is influenced by nutrient status

(A) Western blot of cell lines expressing doxycycline-inducible shGFP or shKRAS cultured with 1μg/mL doxycycline for indicated number of days. (B) Western blot of indicated cell lines expressing shGFP or shKRAS cultured in 4mM or 0.5mM glutamine for 72 hours. (C, D, E) Heatmap of differentially expressed genes for cell lines cultured in (C) 4mM or 0.5mM glutamine for 72 hours (D) cells expressing shGFP or shKRAS cultured in 4mM glutamine or (E) cells expressing shGFP or shKRAS cultured in 0.5mM glutamine for 72 hours. (F) Venn diagram of genes differentially regulated by glutamine deprivation, or by KRAS knockdown in either 4mM or 0.5mM glutamine. (G) Comparison of directionality of expression changes after glutamine deprivation or KRAS knockdown in 0.5mM glutamine. (H) Pathways differentially regulated in 0.5mM glutamine, by KRAS in 0.5mM glutamine, or by both. (I, J) Analysis of overall survival for (I) total cohort of NSCLC patients or (J) the subset with confirmed KRAS mutation with patients were stratified into high or low

expression of the 100 genes regulated by both glutamine deprivation and by KRAS in 0.5mM glutamine. Human lung cancer gene expression data were from the TCGA cohort (http://cancergenome.nih.gov/). Corresponding mutation data for same samples were downloaded from the Xena browser (https://xenabrowser.net/) (see STAR Methods). See also Figure S1.

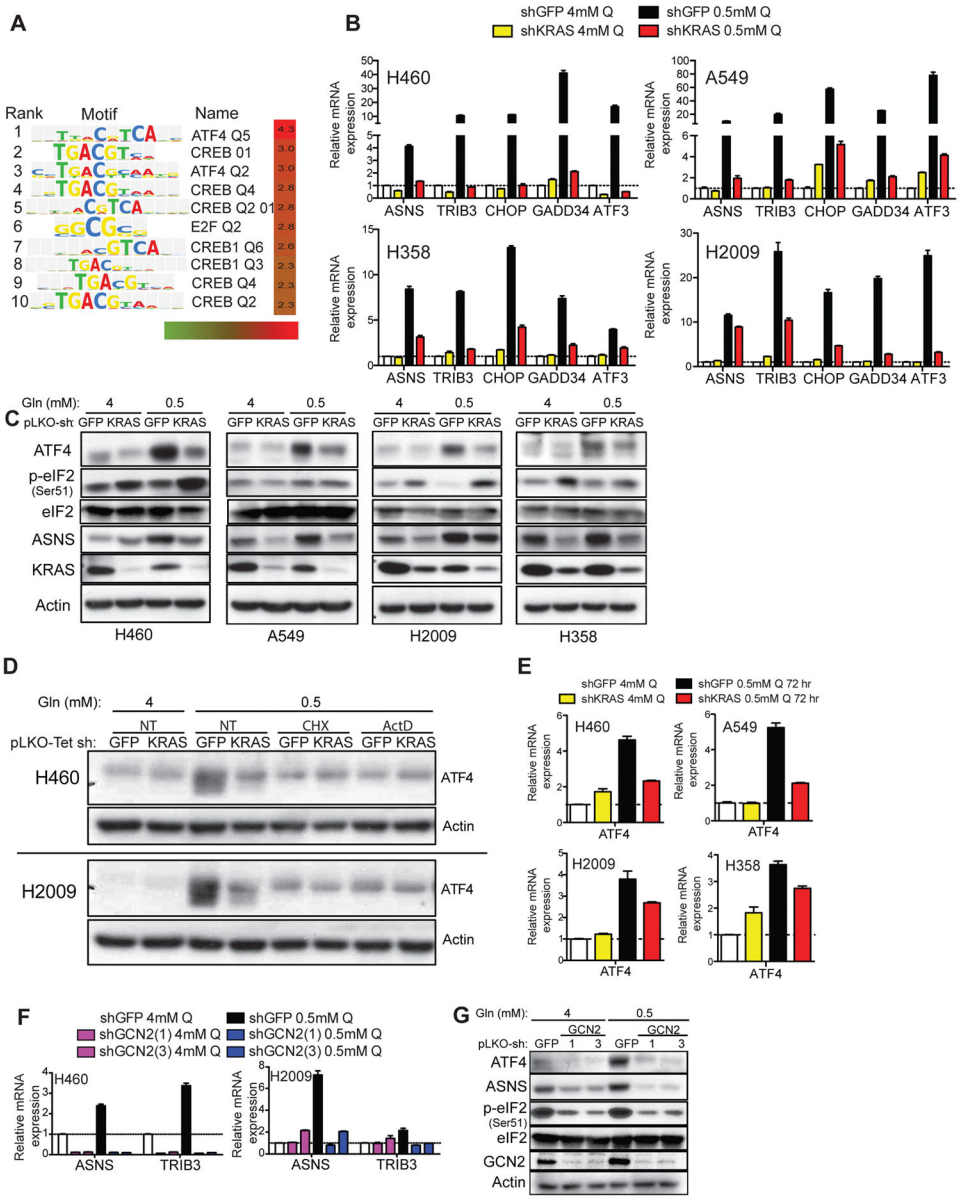

Figure 2. KRAS cooperates with the GCN2-p-eIF2 pathway to induce ATF4

(A) Transcription factors with enriched binding sites in genes differentially regulated by both glutamine deprivation and by KRAS in 0.5mM glutamine. Heat map scales are ranked by −log (p-value). Weighted binding motifs were analyzed and acquired using Transfac 2016.1. (B) RT-qPCR for indicated ATF4 target genes (results are the average of 3 technical replicates) and (C) Western blots for cell lines expressing shGFP or shKRAS in 4mM or 0.5mM glutamine for 72 hours. (D) Western blots of cells expressing shGFP or shKRAS cultured in 4mM or 0.5mM glutamine in the presence of actinomycin D (1ng/mL) or cycloheximide (10μg/mL) where indicated for 12 hrs. (E) RT-qPCR for ATF4 in indicated NSCLC cells expressing shGFP or shKRAS cultured in 4mM or 0.5mM glutamine for 72 hrs (results are the average of 3 technical replicates). (F) RT-qPCR (results are the average of 3 technical replicates) for indicated cells or (G) Western blots for for H2009 cells expressing

shGFP or shGCN2 cultured in 4 or 0.5mM glutamine for 72 hrs. Error bars represent mean +/− SEM. See also Figure S2.

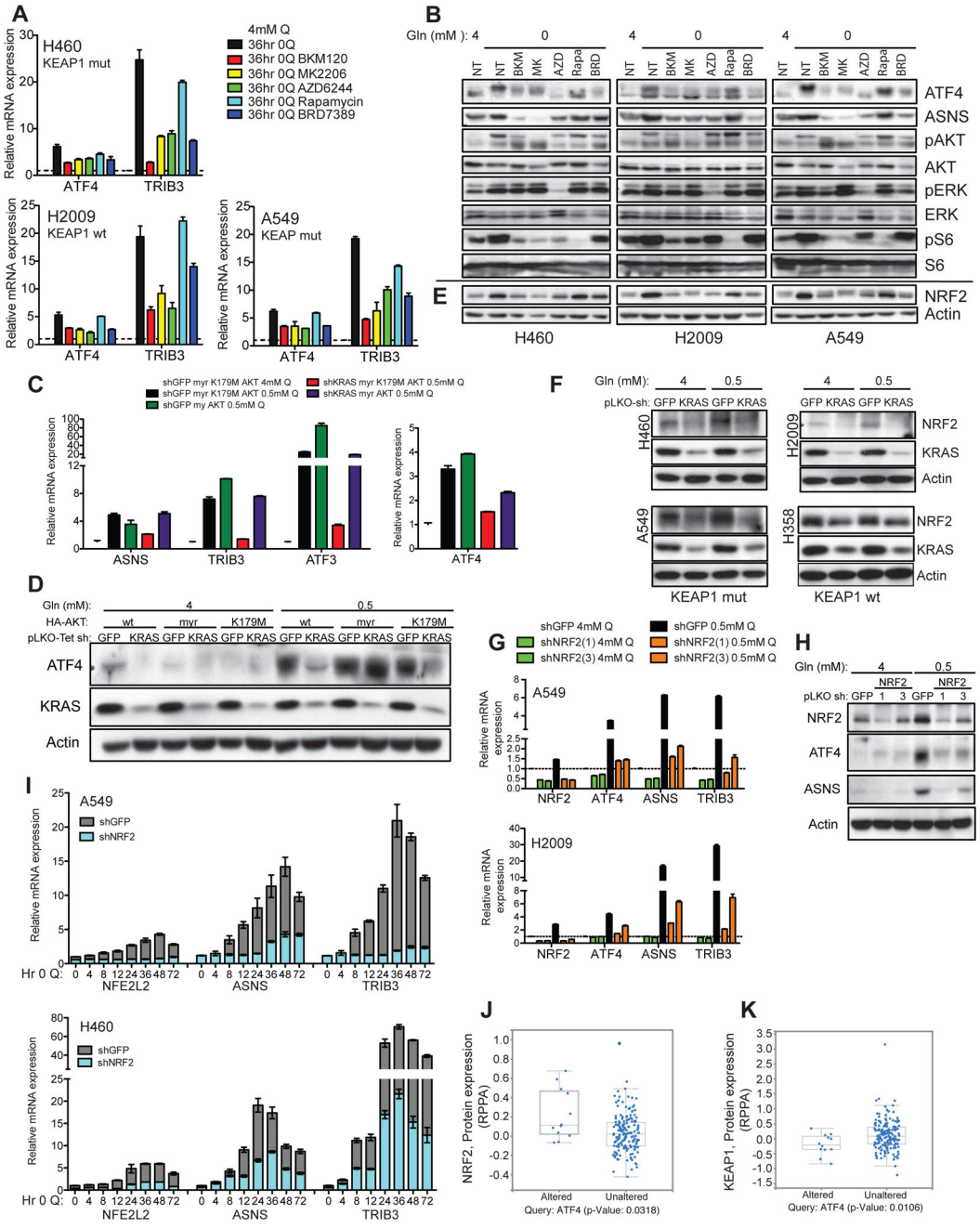

Figure 3. NRF2 is required for KRAS-mediated regulation of ATF4 via PI3K

(A) RT-qPCR (results are the average of 3 technical replicates) and (B) Western blots from cells not-treated (NT), or treated with 5μM BKM120, 5μM MK2206, 10μM AZD6244, 100nM Rapamycin or 10μM BRD7389 for 72 hrs, with glutamine withdrawal for the last 36 hours. (C) RT-qPCR (results are the average of 3 technical replicates) and (D) Western blots for A549 cells expressing shGFP or shKRAS and constitutively active myr-AKT or kinase dead myr-K179M AKT cultured in 4mM or 0.5mM glutamine for 72 hrs. (E) Western blots for NRF2 for experiment described in (B). (F) Western blots of indicated cells expressing shGFP or shKRAS cultured in 4mM or 0.5mM glutamine for 72 hrs. (G) RT-qPCR (results

are the average of 3 technical replicates) and (H) Western blots of H2009 and A549 cells expressing shGFP or shNRF2 cultured in 4mM or 0.5mM glutamine for 72 hrs. (I) RT-qPCR (results are the average of 3 technical replicates) for indicated cells expressing shGFP or shNRF2 at indicated time-points (in hours) after glutamine withdrawal. Protein levels of (J) KEAP1 or (K) NRF2 from lung tumors with altered or unaltered expression of *ATF4* (see Figure S3B) Human lung cancer gene expression and protein data were obtained from the TCGA network (http://cancergenome.nih.gov/). Error bars represent mean +/−SEM. See also Figure S3.

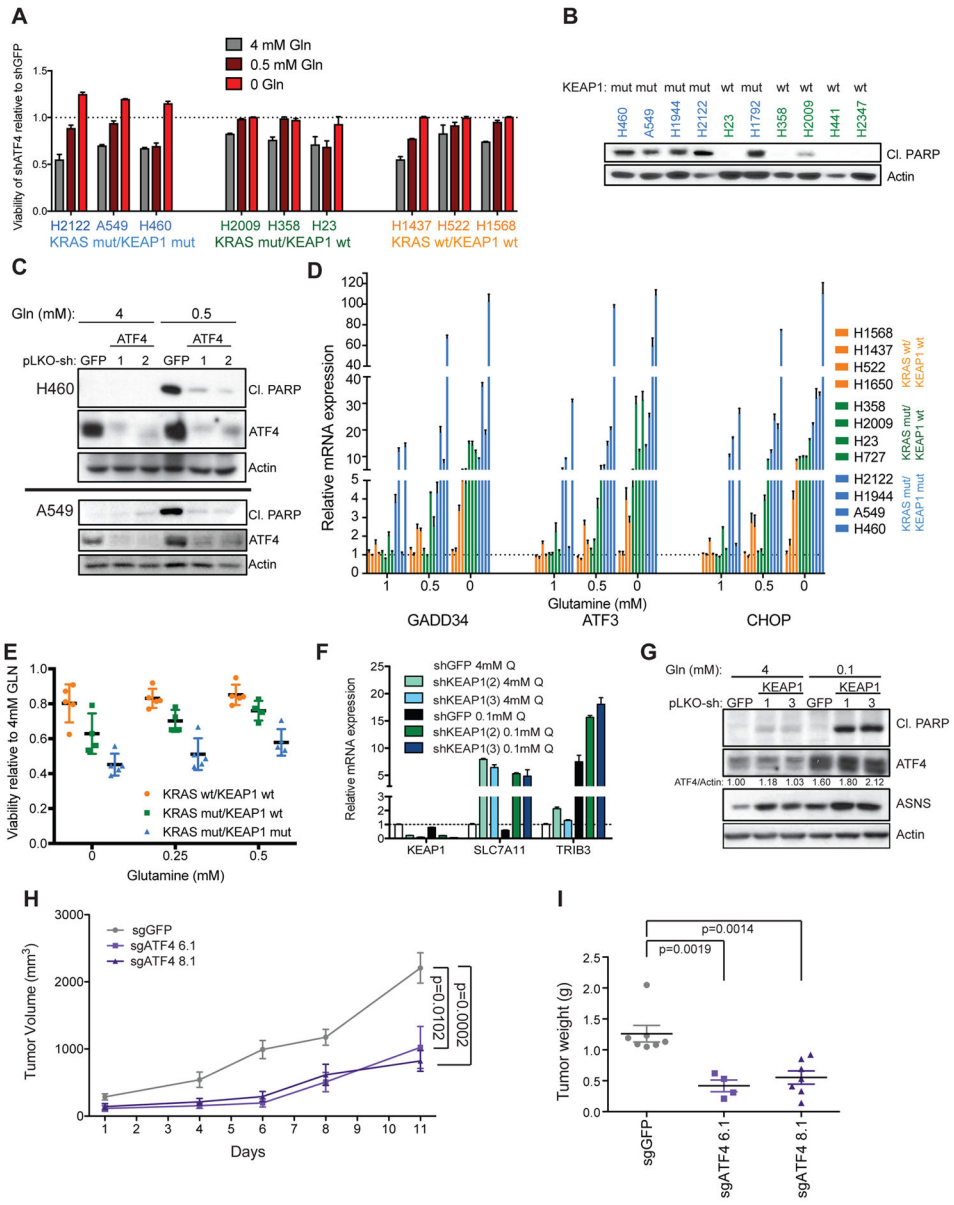

Figure 4. The role of ATF4 is dependent on nutrient status and genetic context

(A) Viability of indicated NSCLC cell lines expressing shATF4 relative shGFP grown in the indicated glutamine concentration for 48 hours (results are the average of 3 technical replicates). (B) Western blots of indicated cells cultured cultured in 0.5mM glutamine for 72 hrs. (C) Western blots of indicated cells expressing shGFP or shATF4 cultured in 4 mM or 0.5mM glutamine for 72 hrs. (D) RT-qPCR for ATF4 targets from cells with wild-type (wt) KRAS and wt KEAP1, an oncogenic mutation (mut) in KRAS and wt KEAP1, or KRAS mut and KEAP1 mut cultured in indicated glutamine concentrations relative to cells cultured in 4mM glutamine (results are the average of 3 technical replicates). (E) Viability of cell lines bearing the indicated mutations cultured in 0, 0.25, or 0.5 mM glutamine for 48 hrs relative to 4mM glutamine. Each data point represents the average of 3 technical replicates from one cell line. (F) RT-qPCR (results are the average of 3 technical replicates) and (G)

Western blots of H358 cells expressing shGFP or shKEAP1 cultured in 4mM or 0.1mM glutamine for 72 hrs. (H) Growth curves, and (I) final tumor weights of H460 xenograft tumors with CRISP-Cas9 mediated deletion of ATF4 (sgGFP n=7; sgATF4.6 n=4; sgATF4.8 n=7). Error bars represent mean +/−SEM; p-values were calculated by a two-tailed *t*-test. See also Figure S4.

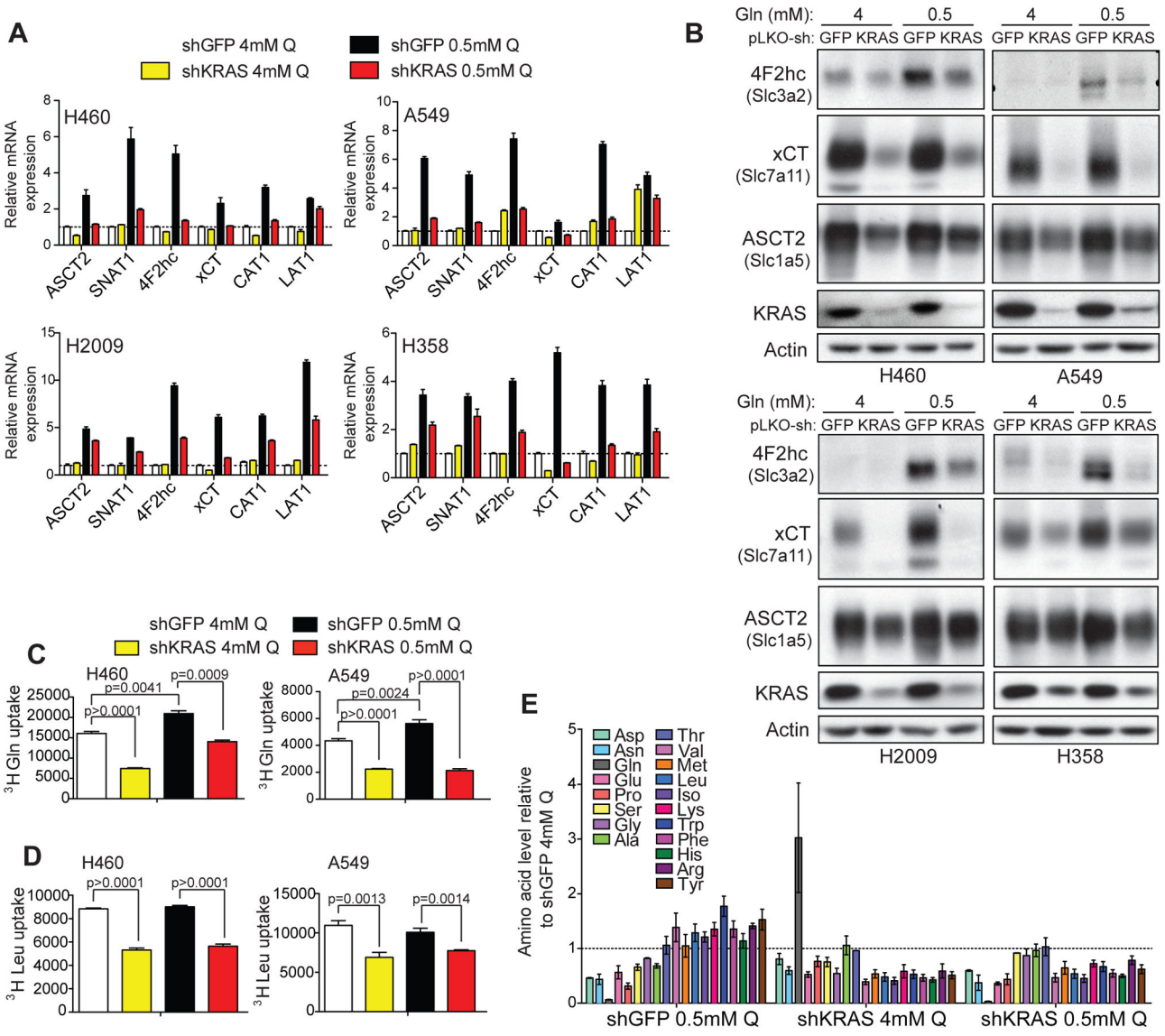

Figure 5. KRAS regulates amino acid transport and metabolism during nutrient stress

(A) RT-qPCR (results are the average of 3 technical replicates) and (B) Western blots for amino acid transporters in cell lines expressing dox-inducible shGFP or shKRAS cultured in 4mM or 0.5mM glutamine for 72 hrs. (C) ^{3}H-Glutamine and (D) ^{3}H-leucine uptake measured by scintillation count in A549 or H460 cell lines expressing shGFP or shKRAS cultured in 4mM or 0.5mM glutamine for 72 hrs (normalized to cell number). Results are the average of three biological replicates. (E) Intracellular amino acid levels in H460 cells expressing shGFP or shKRAS cultured in 4mM or 0.5mM glutamine for 72 hrs (normalized to cell number). Results are the average of 2 biological replicates. Error bars represent mean +/−SEM; p-values were calculated by a two-tailed *t*-test. See also Figure S5.

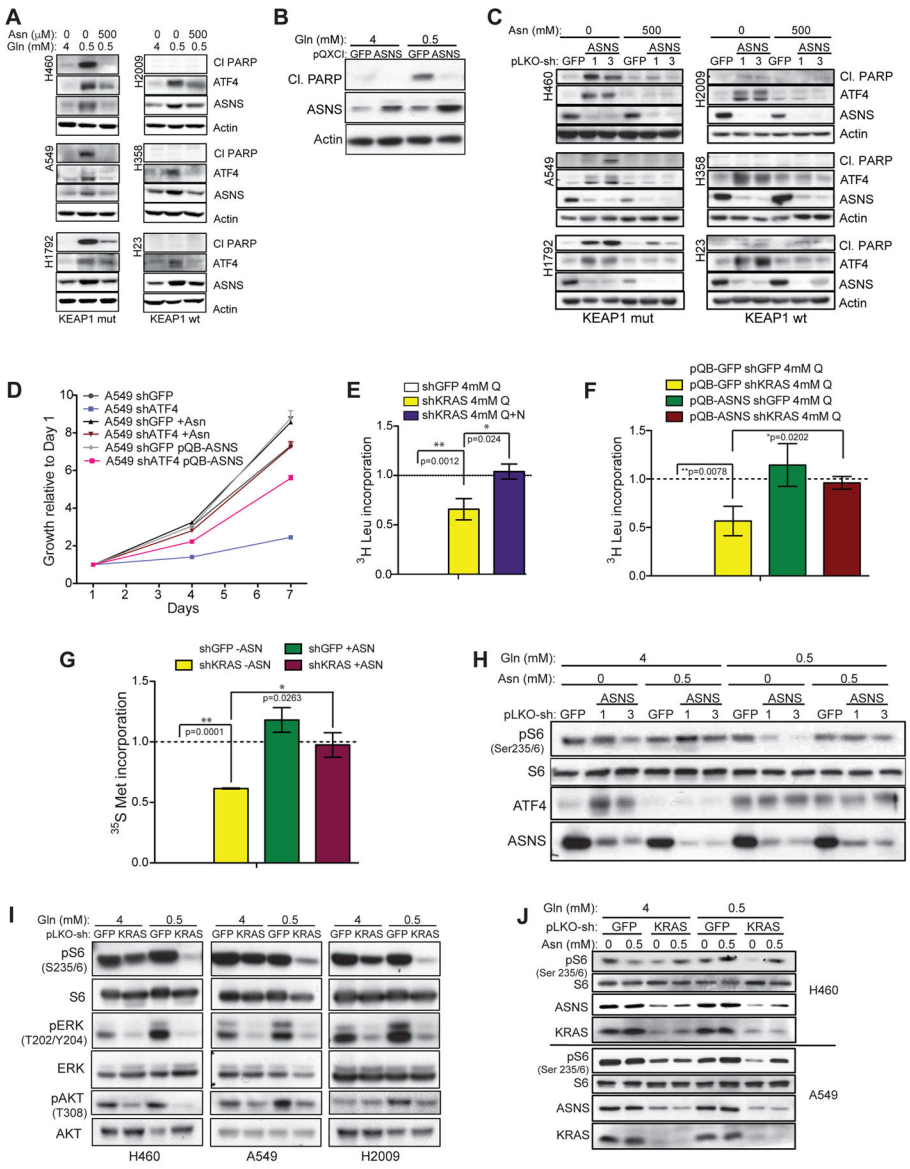

Figure 6. KRAS contributes to protein biosynthesis and supports mTORC1 signaling via regulation of ASNS

(A) Western blots of indicated NSCLC cells cultured in 4mM or 0.5mM glutamine for 72 hrs with addition of 0.5mM asparagine where indicated. (B) Western blots of H460 cells expressing pQB-GFP or pQB-ASNS cultured in indicated concentration of glutamine for 72 hrs. (C) Western blots of indicated NSCLC cells expressing shGFP or shASNS cultured in 4mM glutamine with addition of 0.5mM asparagine where indicated for 72 hrs. (D) Growth curves of A549 cells expressing shGFP or shATF4 cultured in 4mM glutamine DMEM with or without asparagine (Asn) for 72 hrs or with overexpression of ASNS (pQB-ASNS). Results are average of 3 biological replicates. (E, F) Protein synthesis rates (incorporation of ^{3}H-Leucine into peptides) for H460 cells expressing shGFP or shKRAS cultured in 4mM glutamine with (E) addition of 500μM asparagine where indicated or (F) over-expression of ASNS. Results are average of 3 biological replicates. (G) Protein synthesis rates

(incorporation of ^{35}S-Methionine) for H460 cells expressing shGFP or shKRAS cultured in 4mM glutamine with addition of 500μM asparagine where indicated for 96 hours. Results are average of 3 biological replicates. (H) Western blots of H460 cells expressing shGFP or shASNS cultured in 4mM or 0.5mM glutamine for 72 hrs with addition of 0.5mM asparagine where indicated. (I) Western blots of H460 and A549 cells expressing shGFP or shKRAS in 4mM or 0.5mM glutamine for 72 hrs. (J) Western blots of H460 and A549 cells expressing shGFP or shKRAS in 4mM or 0.5mM glutamine for 72 hrs with addition of 0.5mM asparagine where indicated. Error bars represent mean +/− SEM. p-values were calculated by a two-tailed *t*-test; *p<0.05, **p<0.001. See also Figure S6.

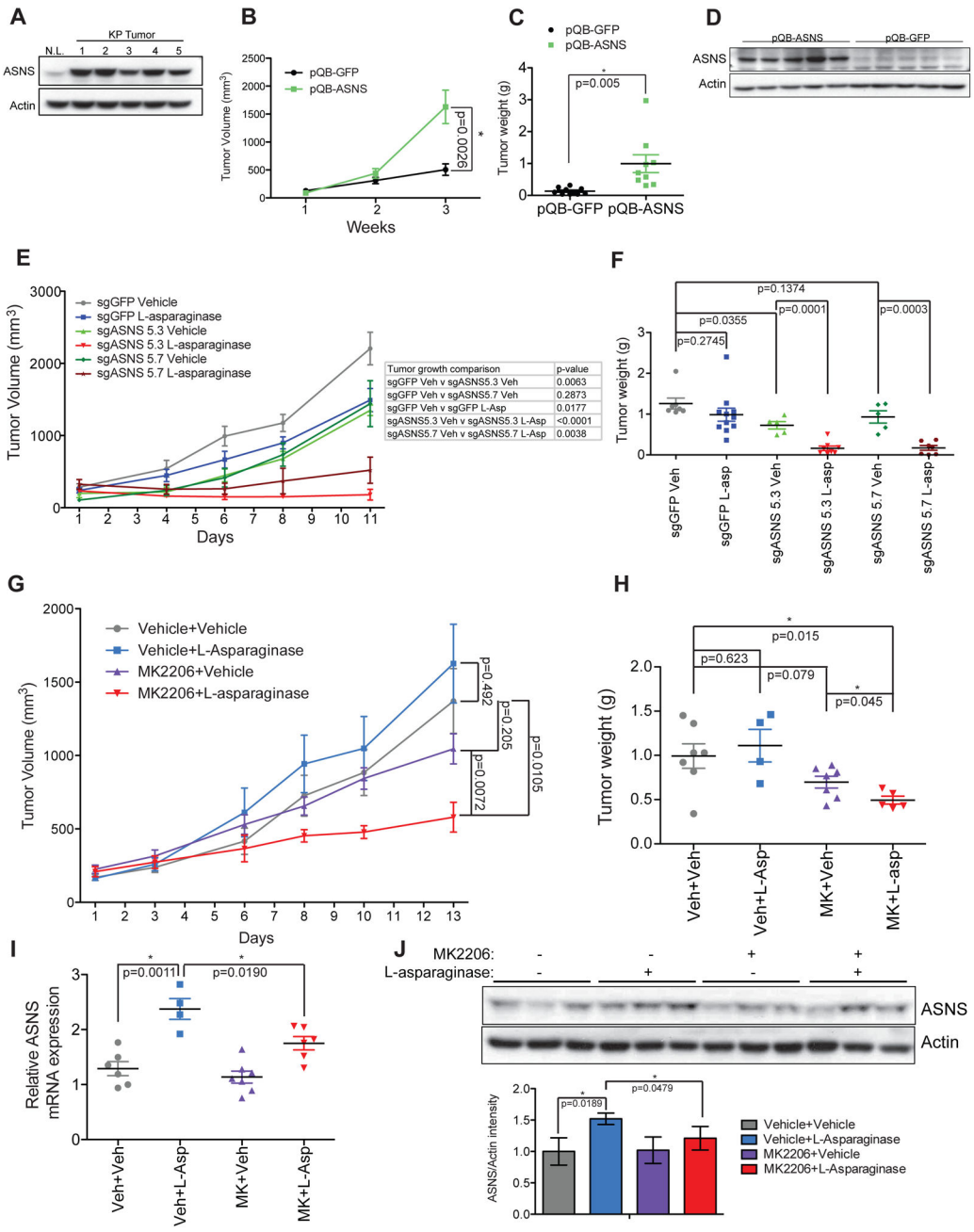

Figure 7. Asparagine synthetase is rate-limiting for tumorigenesis

(A) Western blots of ASNS in lung tumors dissected from KRAS-LSL^{G12D};p53$^{fl/fl}$ mice 12 weeks after adenoviral Cre administration. (B) Growth curves, and (C) final tumor weights of A549 xenograft tumors expressing pQB-GFP (n=5) or pQB-ASNS (n=5). (D) Western blots of tumors from (B, C). (E) Growth curves and (F) final tumor weights of H460 xenograft tumors with CRISPR-Cas9 mediated deletion of ASNS treated with vehicle or L-asparaginase (L-Asp) (sgGFP+Vehicle n=7; sgGFP+L-Asp n=11; sgASNS5.3+Vehicle n=5; shASNS5.3+L-Asp n=8; sgASNS5.7+Veh n=5; shASNS5.7+L-Asp n=7). (G) Growth curves and (H) final tumor weights of H460 xenograft tumors treated with vehicle (n=7), L-

asparaginase (3UI/kg daily) (n=4), MK2206 (120 mg/kg 3X/week) (n=7) or both (n=5). (I) RT-qPCR and (J) Western blots of tumors dissected from (G, H) for ASNS levels. Error bars represent mean +/− SEM. p-values were calculated by a two-tailed *t*-test: *p<0.05, **p<0.001. See also Figure S7.

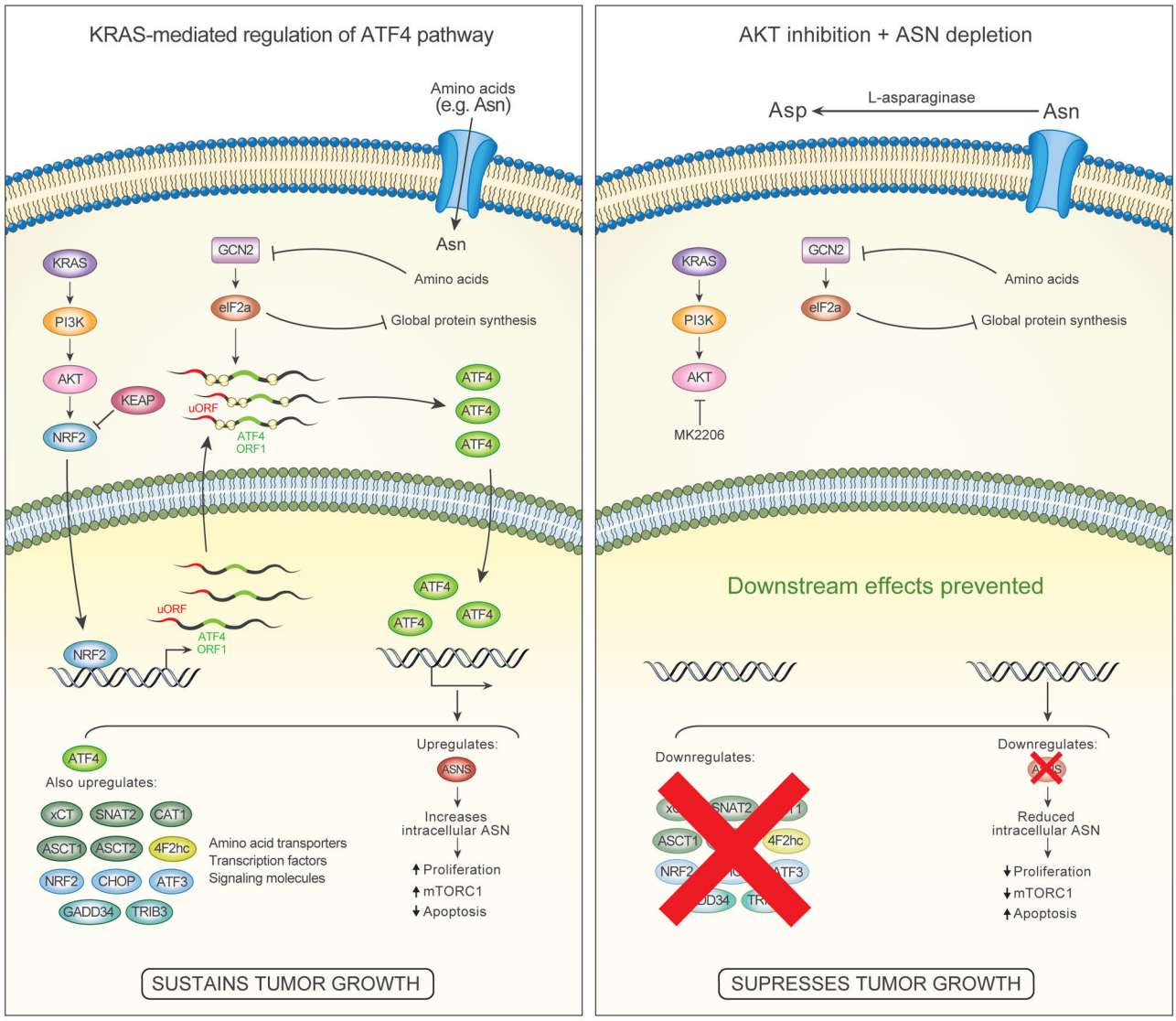

Figure 8. Mechanisms involved in regulation of amino acid metabolism by oncogenic KRAS

(Left) KRAS enhances ATF4 mRNA levels through PI3K-AKT mediated NRF2 up-regulation. ATF4 translation is stimulated during nutrient deprivation by activation of the GCN2-p-eIF2 pathway, resulting in up-regulation of ATF4 protein levels, and ATF4 target genes. ASNS is an ATF4 target gene responsible for asparagine biosynthesis, which contribute to protein synthesis, suppression of apoptosis and up-regulation of mTORC1. (Right) When AKT is inhibited, abrogating ATF4 up-regulation during nutrient deprivation, and extracellular asparagine is depleted by the chemotherapeutic, L-asparagine, cells are asparagine starved, and tumor growth is suppressed.

KEY RESOURCES TABLE

REAGENT or RESOURCE	SOURCE	IDENTIFIER
Antibodies		
Mouse monoclonal anti-KRAS	Santa Cruz Biotechnology	Cat# sc-30, RRID:AB_62765
Mouse monoclonal anti-ASNS	Santa Cruz Biotechnology	Cat# sc-365809, RRID:AB_10843357
Rabbit monoclonal anti-ASNS	LifeSpan Biosciences	Cat# LS-C49697 (discontinued)
Rabbit monoclonal anti-ATF4	Cell Signaling Technologies	Cat# 11815, RRID:AB_2616025
Rabbit monoclonal anti-phospho-eIF2	Cell Signaling Technologies	Cat# 3597, RRID:AB_390740
Rabbit monoclonal anti-eIF2	Cell Signaling Technologies	Cat# 5324, RRID:AB_10692650
Rabbit monoclonal anti-GCN2	Cell Signaling Technologies	Cat# 3302, RRID:AB_2277617
Rabbit monoclonal anti-ASCT2	Cell Signaling Technologies	Cat# 8057, RRID:AB_10891440
Rabbit monoclonal anti-4F2hc	Cell Signaling Technologies	Cat# 13180
Rabbit monoclonal anti-NRF2	Cell Signaling Technologies	Cat# 12721
Rabbit monoclonal anti-xCT	Cell Signaling Technologies	Cat# 12691
Rabbit monoclonal anti-phospho AKT (S473)	Cell Signaling Technologies	Cat# 4060, RRID:AB_2315049
Rabbit monoclonal anti-AKT	Cell Signaling Technologies	Cat# 9272, RRID:AB_329827
Rabbit monolonal anti-phospho ERK (S202/Y204)	Cell Signaling Technologies	Cat# 4370, RRID:AB_2315112
Rabbit monoclonal anti-ERK	Cell Signaling Technologies	Cat# 4695, RRID:AB_390779
Rabbit monoclonal anti-phospho-S6 (S235/236)	Cell Signaling Technologies	Cat# 4858, RRID:AB_916156
Rabbit monoclonal anti-S6	Cell Signaling Technologies	Cat# 2217, RRID:AB_331355
Rabbit monoclonal anti-Cleaved PARP	Cell Signaling Technologies	Cat# 5625, RRID:AB_10699459
Mouse monoclonal anti-b-actin	SIGMA	Cat# A2228, RRID:AB_476697
Bacterial and Virus Strains		
Adenoviral Cre	University of Iowa Viral Vector Core Facility	Cat# VVC-U of Iowa-5
Biological Samples		
Leunase/L-asparaginase	Kyowa Hakko Kirin	N/A
Chemicals, Peptides, and Recombinant Proteins		
Doxycycline	SIGMA	Cat# D9891; CAS: 24390-14-5
Puromycin	ThermoFisher	Cat# A1113803; CAS: 53-79-2
BKM120, PI3K inhibitor	Selleck Chemicals	Cat# S2247; CAS: 944396-07-0
MK2206, AKT inhibitor	Selleck Chemicals	Cat# S1078; CAS: 1032350-13-2
AZD6244, MEK inhibitor	Selleck Chemicals	Cat# S1008; CAS: 606143-52-6
Rapamycin, mTOR inhibitor	Selleck Chemicals	Cat# S1039; CAS: 53123-88-9

REAGENT or RESOURCE	SOURCE	IDENTIFIER
BRD7389, RSK inhibitor	Tocris	Cat# 4037; CAS: 376382-11-5
Asparagine	SIGMA	Cat# A0884; CAS: 70-47-3
Glutamine	SIGMA	Cat# G3126; CAS: 56-85-9
MTT (Thiazolyl Blue Tetrazolium Bromide)	SIGMA	Cat# M2128; CAS: 298-93-1
Trizol	ThermoFisher	Cat# 15596026
MG-132	SIGMA	Cat# M8699
Actinomycin D	SIGMA	Cat# A1410
Cycloheximide	SIGMA	Cat# C7698
^{3}H-Leucine	Perkin Elmer	NET135H250UC
^{3}H-Glutamine	Perkin Elmer	NET551250UC
^{35}S-Protein Labeling Mix	Perkin Elmer	NEG072002MC
Critical Commercial Assays		
BCA Kit	ThermoFisher	Cat# 23225
RNeasy Mini Kit	QIAGEN	Cat# 74104
Maxima First Strand cDNA Synthesis Kit	ThermoFisher	Cat# K1671
PerfeCTa SYBR Green SuperMix	Quanta Biosciences	Cat# 95054
Deposited Data		
shGFP v shKRAS in 4v0.5mM Gln microarray data	This study	GEO: GSE81644
Lung adenocarcinoma expression data with ATF4 alterations (TCGA, Nature 2014)	TCGA, via cBioPortal	http://www.cbioportal.org/
Lung cancer gene expression data for analysis of Kras expression genesets	source: http://gdac.broadinstitute.org/runs/stddata__2016_01_28/data/LUAD/20160128/ filename: gdac.broadinstitute.org_LUAD.Merge_rnaseqv2__illuminahiseq_maseqv2__unc_edu__Level_3__RSEM_genes_normalized__data.Level_3.2016012800.0.0.tar.gz file hash: 4C36EEC3F6DF75630292C5A569CFC8F4 source: extracted file name: LUAD.rnaseqv2__illuminahiseq_rnaseqv2__unc_edu__Level_3__RSEM_genes_normalized__data.data.txt hash value: 360BB0672CED057CCAFEBF225E79F07B	https://gdac.broadinstitute.org/
Lung cancer somatic mutation data (KRAS)	Somatic mutation: https://xenabrowser.net/datapages/?dataset=TCGA/TCGA.LUAD.sampleMap/mutation_broad&host=https://genome-cancer.ucsc.edu:443/proj/public/xena filename: mutation_broad hash value: 15D519F1401694D3AC63B9AFB8ACF599	(https://xenabrowser.net/
Cell Lines		
Human: NCI-H358 (Male)	ATCC	CRL-5807
Human: NCI-H1792 (Male)	ATCC	CRL-5895
Human: NCI-H23 (Male)	ATCC	CRL-5800
Human: NCI-H1944 (Female)	ATCC	CRL-5907
Human: NCI-H2122 (Female)	ATCC	CRL-5985
Human: NCI-H1568 (Female)	ATCC	CRL-5876
Human: NCI-H727 (Female)	ATCC	CRL-5815

REAGENT or RESOURCE	SOURCE	IDENTIFIER
Human: NCI-H1437 (Male)	ATCC	CRL-5872
Human: NCI-H522 (Male)	ATCC	CRL-5810
Human: NCI-H1650 (Male)	ATCC	CRL-5883
Human: NCI-H441 (Male)	ATCC	HTB-174
Human: NCI-H2347 (Female)	ATCC	CRL-5942
Human: NCI-H460 (Male)	ATCC	HTB-177
Experimental Models: Organisms/Strains		
Mouse strain: NOD.Cg-*Prkdc*^{scid} *Il2rg*^{tm1Wjl}/SzJ (NSG)	The Jackson Laboratory	Cat# 005557
Mouse strain: Lox-stop-lox-Kras^{G12D} (Jackson et al., 2001); Trp53$^{fl/fl}$ (Jonkers et al., 2001)		
Oligonucleotides		
See Table S4		N/A
Recombinant DNA		
MCB306	Han et al., 2017	AddGene Plasmid #89360
lentiCas9	Sanjana et al., 2014	AddGene Plasmid #52962
pQXCI-Blast	Campeau et al., 2009	AddGene Plasmid #17400
pDONR221-ASNS	ASU DNA repository	Cat# HsCD00045070
pLNCX-wt AKT, pLNCX-myr-AKT, pLNCX-myr K179M AKT	Ramaswamy et al., 1999	AddGene Plasmids #9004, 9005, 9006
pLKO.1-Tet	Wiederschain et al., 2009	AddGene Plasmid #21915
Software and Algorithms		
N/A		
Other		
N/A		